THESIS FOR THE DEGREE OF LICENTIATE OF ENGINEERING

Morphological and structural analysis of dialcohol cellulose fibres: a multi-length scale approach

Nivedhitha Venkatraman

Industrial and Materials Science

CHALMERS UNIVERSITY OF TECHNOLOGY

Gothenburg, Sweden 2024

Morphological and structural analysis of dialcohol cellulose fibres: a multi-length scale approach
NIVEDHITHA VENKATRAMAN

Technical report no IMS-2024-16
Industrial and Materials Science
Chalmers University of Technology
SE-412 96 Gothenburg
Sweden

Cover: Image illustrating a morphology of modified fibre, by Nivedhitha Venkatraman.
Printed by Chalmers Digitaltryck
Gothenburg, Sweden 2024

Morphological and structural analysis of dialcohol cellulose fibres: a multi-length scale approach

NIVEDHITHA VENKATRAMAN

Industrial and Materials Science IMS

Chalmers University of Technology

Abstract

There is an urgent need for a transition from the consumption of fossil-based resources to sustainable and renewable counterparts. Bio-based alternatives like cellulose are promising materials to replace synthetic polymers. However, cellulosic materials requires some type of chemical modification to facilitate processing into complex structures. One way to overcome this challenge is to partly modify cellulose in cellulose fibres to dialcohol cellulose, which can be softened by both temperature and moisture. This thesis explores the swelling behaviour of partially modified dialcohol cellulose fibres (bleached softwood kraft pulp) of different degree of modification (DOM); from the nanoscale to the microscale using characterisation tools such as x-ray scattering and optical microscopy. Wide-angle x-ray scattering reveals the structures inside the fibre wall at the Angstrom level, while small-angle x-ray scattering (SAXS) provides information about the morphologies at the nanometre level. The SAXS results give an estimation of the distance between nanofibrils and the swelling of nanofibril bundles. The SAXS results show that with an increase in DOM, the SAXS peak shifts from ~5 nm (for unmodified, bench-dried cellulose fibres) to ~11 nm (for bench-dried, dialcohol cellulose fibres with 51% DOM). In addition, at the fibre level, microscopic studies indicate that when fibres are partially modified, a mild ballooning in the swollen fibres is observed (for never-dried fibres of ~25% DOM) with an average fibre width of 35 ± 9 μm to 58 ± 24 μm (for never-dried fibres of ~50% DOM). Furthermore, the water retention value ranged between 1.7-6.3 g_{water}/g_{fibre}, depending on degree of modification. Interestingly, there was a linear correlation between the swelling propensity from the water retention values and the nano-swelling from the SAXS peaks, indicating that the SAXS peaks correlate to the microscopic swelling of the fibre wall.

List of Publications and Presentations

This thesis is based on the following appended manuscripts:

I. **Dialcohol cellulose fibres and the effect of their modifications on the structure of the fibres: a small- and wide-angle x-ray scattering study**
Nivedhitha Venkatraman, Katarina Jonasson, Hampus Karlsson, Johanna Sjölund, Michal Strach, Giada Lo Re, Lars Evenäs, Per A. Larsson, Anette Larsson
Manuscript

II. **The effect of the degree of modification of dialcohol cellulose on the morphology and swelling of cellulose fibres**
Nivedhitha Venkatraman, Katarina Jonasson, Giada Lo Re, Per A. Larsson, Anette Larsson
Manuscript

Contribution Report

The author of this thesis has made the following contributions to the publications included:

Paper I: First author. Developed the concept and experimental design in collaboration with supervisors. Performed most of the experimental work except for the DNP-NMR. Wrote the first draft of the paper. Revised the paper in collaboration with co-authors.

Paper II: First author. Developed the concept and experimental design in collaboration with all co-authors. Performed most of the experimental work, except for the molecular weight analysis. Analyzed and interpreted results in collaboration with supervisors. Wrote the first draft of the paper. Revised the paper in collaboration with all co-authors.

Abbreviations and Symbols

BD	Bench Dried
BDDJ	Britts Dynamic Drainage Jar
CLSM	Confocal Laser Scanning Microscopy
CNFs	Cellulose Nanofibrils
DAC	Dialdehyde Cellulose
DALC	Dialcohol Cellulose
DIC	Differential Interference Contrast
DOM	Degree of Modification
DP	Degree of Polymerisation
EFBs	Elementary Fibril Bundles
FITC	Fluorescein Isothiocyanate
MAXS	Medium Angle X-ray Scattering
Mw	Weight-Average Molecular Weight
ND	Never Dried
NMR	Nuclear Magnetic Resonance
OM	Optical Microscopy
PM	Polarisation Microscopy
RW	Rewetted
SAXS	Small Ange X-ray Scattering
WAXS	Wide Angle X-ray Scattering
WRV	Water Retention Value

Table of Contents

1. INTRODUCTION 1

2. BACKGROUND 3

2.1 Cellulose in wood 3

2.2 Chemical composition and hierarchical structure of cellulose in wood 4

2.3 Polymorphic crystalline structure in cellulose 5

2.4 Cellulosic fines 6

2.5 Dialcohol cellulose (DALC) fibres 7

2.6 Structure of cellulose using x-ray scattering techniques 8

2.7 Morphology of cellulose fibres using microscopy techniques 10

2.7.1 Polarisation microscopy 10

2.7.2 Differential interference contrast microscopy 11

2.7.3 Confocal laser scanning microscopy 12

3. MATERIALS AND METHODS 15

3.1 Materials – preparation of dialcohol cellulose 15

3.1.1 Materials 15

3.1.2 Preparation of dialcohol cellulose fibres 15

3.2 Methods of characterisation 17

3.2.1 Fibre size analysis 17

3.2.1.1 Gravimetric determination of fines 17

3.2.1.2 Automated optical fibre analysis 18

3.2.2 Analysis of water content in the fibres 18

3.2.2.1 Water retention value – quantitative 18

3.2.2.2 Optical microscopy and image analysis - qualitative 19

3.2.2.3 Confocal laser scanning microscopy - qualitative 19

3.2.2 X-ray scattering techniques 20

4. RESULTS AND DISCUSSION 23

4.1 Assessment of fines and degree of modification for partially modified DALC 23

4.2 Swelling propensity of DALC with different degrees of modification at different length scales 25

4.2.1 Influence of modification on the structure of fibre at the nanoscale 25

4.2.1.1 WAXS studies of DALC fibres with different DOMs and sample treatments 25

4.2.1.2 SAXS studies of DALC fibres with different DOM 27

4.2.2 Swelling propensity at the microscale for different degrees of modification 30

4.2.2.1 Water retention value for the different DALC samples 30

4.2.2.2 Optical Microscopy 31

4.3 Correlation of swelling propensity between the nanometre scale and the micrometre scale. 38

5. CONCLUSION 39

6. ACKNOWLEDGMENTS 41

7. REFERENCES 42

1. Introduction

The development of synthetic polymers, often called plastics has steadily increased since the early 1950s and is incorporated into most people's lives today [1]. This is exemplified by a revolution in the packaging industry, where plastics increase the shelf life of groceries and hence reduce food waste. Furthermore, the use of single-use medical equipment and devices has facilitated improved hygiene in the medical field, enhancing the quality of life for humans [2]. Despite the positive contributions of plastics in society, there are nevertheless drawbacks related to usage of products derived from fossil fuels, pollution caused by the littering of plastic, and the accumulation of plastics in nature and in the oceans. The management of polymer waste and the reduction of plastic consumption is crucial. The plastics used today in packaging and single-use products could be replaced by more sustainable materials, which would be beneficial in terms of reducing environmental pollution.

The demand for sustainability in industry and society emphasizes the need for low-cost, eco-friendly materials with the potential for high-volume production. There has been a pressing need for a transition from excessive consumption of fossil-based resources to finding suitable renewable and bio-based alternatives. In 2022, European plastic production amounted to 59 tonnes, 54 of which were converted into plastic products and parts by European companies. Plastic packaging constituted 39% of the converted plastic products. Bio-based plastics represent less than 1% (0.4 tonnes) of the total European plastic production [3].

Cellulose from wood is of special interest to the Swedish forest industry [4], in part because two thirds of Sweden is covered by forest (according to 2011 statistics) [5]. With the pressing need for a transition from the excessive consumption of fossil-based resources to suitable renewable and bio-based alternatives, cellulose could provide a suitable alternative for the future.

One of the major limitations of thermoprocessing of native cellulose is that, upon heating, it degrades before it significantly softens. To overcome this limitation, native cellulose can be chemically modified, for example by partially modifying the cellulose fibres to dialcohol cellulose (DALC) fibres. These fibres exhibit high ductility and thermoplastic features [6-10]. Recent studies demonstrated that DALC fibres can be melt-processed by twin-screw extrusion and subsequent injection molding using only water as a plasticizer [11], eliminating the use of polymer additives to preserve recyclability. but there is not yet a detailed mechanistic understanding of how only the DALC fibres, but not unmodified fibres, can be extruded by using water as a plasticizer.

With an effort to facilitate the upscaling of melt-processability using the least amount of water, this thesis aims to explore the morphology and structural changes of the partially modified DALC fibres in the presence and absence of water.

The thesis has the following scientific questions:

- What are structural changes with different degrees of modifications (DOMs) of DALC at the Angstrom to nanometre to micrometre scales?
- How does the drying history of the fibres alter the structure and morphology of these modified DALC fibres?

2. Background

2.1 Cellulose in wood

Cellulose is a linear polymer containing repeating glucose units. These glucose units are connected by β-1,4 glycosidic linkages. Depending on the source, the degree of polymerisation of cellulose is ~14,000 in its native state and 2,500 after a mild delignification [12, 13]. The linear structure of a cellulose chain consisting of a reducing-end glucose that contains an anomeric carbon (C1) and a non-reducing-end glucose consisting of hydrogen and a hydroxy group on the C4 carbon is shown in Figure 1.

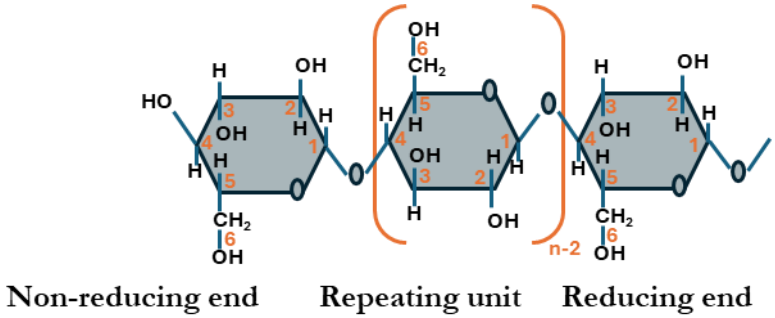

Figure 1. Cellulose polymer chain with glucose units linked by β-(1,4) glycosidic linkages [14].

The cellulose chains organize themselves into nanofibrils that in turn arrange into aggregates or bundles, with nanofibril diametres ranging of 3–5 nm, depending on the source [15-17]. The nanofibril bundles can be a few tens of nanometres depending on the source of raw material, the pulping procedure and the drying history [16, 18, 19]. Nanofibrils can be arranged in 3 × 3 nanofibril bundles as exemplified in Figure 2. Note that 3 × 3 nanofibril bundles are considered for illustration purposes only. In some cases, in the literature, these nanofibril bundles

are depicted differently, e.g., by 4 × 4 nanofibrils [20-22]. Additionally, these nanofibril bundles are alternatively denoted either as elementary fibril bundles because they constitute the basic elementary structure or as "microfibril bundles" [20, 21, 23-28].

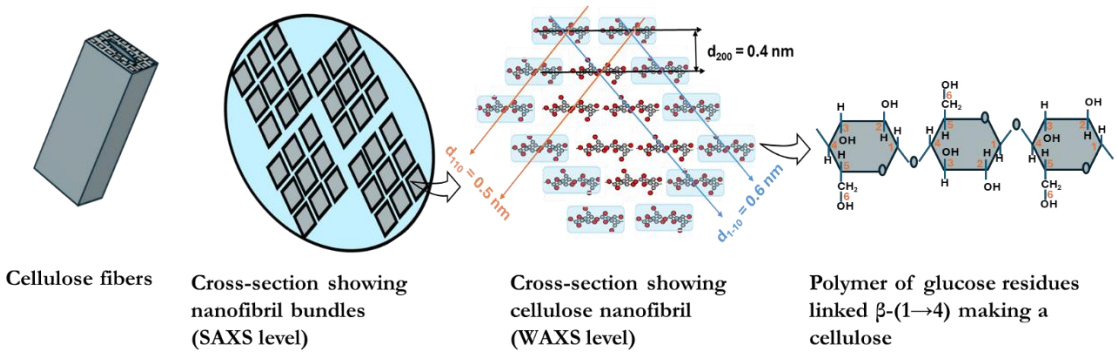

Figure 2. Representative schematics of the hierarchical structure of cellulose fibres down to the molecular structure of the cellulose chain, which can be observed using different x-ray scattering techniques [20, 21].

2.2 Chemical composition and hierarchical structure of cellulose in wood

The cell walls in wood are composed of several layers with different thicknesses that depend on the plant growth cycle (late or early wood). The plant cell types, and hence shape and cell thickness, are different for softwoods and hardwoods. Scandinavian softwood fibres are 2–4 mm in length and roughly 30 μm in width [29]. Regardless of the origin of the fibre, some common hierarchical structures can be recognized. The outer layer is the primary wall followed by the secondary wall. The secondary wall consists of three layers: a thin outer layer S1, an inner layer S3, and a thick middle layer S2 (schematically illustrated in Figure 3). These layers are built up by nanofibrils and bundles of nanofibrils, between which lignin and hemicelluloses are present. The nanofibrils wind around the fibre axis in either an S-helix (counterclockwise) or a Z-helix (clockwise) [30]. The primary wall is very thin, ~0.1 μm, and the nanofibrils are primarily randomly oriented [31]. The angles formed by the nanofibrils in the S1, S2, and S3 layers with respect to the fibre axis

are ~50–70° in the S1 layer, 5–10° for the latewood and ~20–30° for earlywood in the S2 layer, and 50–90° in S3 layer [23]. The thickness of the S1 layer is 0.2–0.3 μm and the nanofibrils form either a Z-helix or S-helix. The thickness of S2 is ~1 μm in earlywood and ~5 μm in latewood. The S3 layer thickness is ~0.1 μm and consists of several lamellae that contain nanofibrils in both Z-helices and S-helices, similar to the S1 layer. The higher the nanofibril angles in the fibres of early wood, the higher the strength in the direction they are aligned. The S2 layer is the thickest and consists of about 50 times more material than the S1 and S3 layers and is arranged in a helical structure [23-25, 31]. S2, being the thickest layer, is also the main contributor to swelling and most other fibre properties. In particular, it has been shown that the primary moisture-induced deformations and swelling occur in the S2 layer and the swelling takes place anisotropically in the transverse direction of the fibre wall [32].

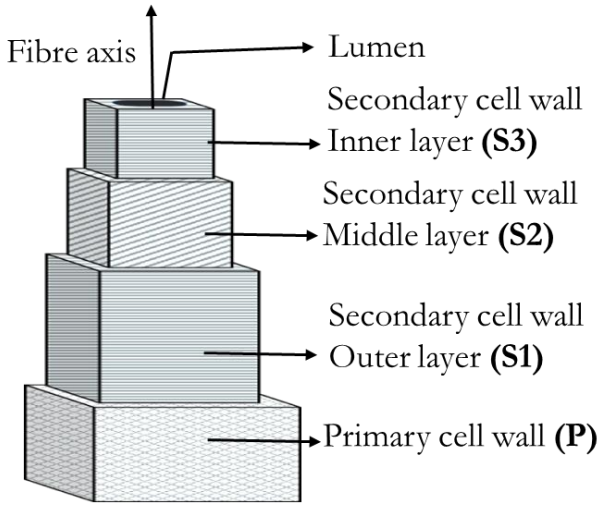

Figure 3. Schematic illustration of the ultrastructure of cellulose fibres with different secondary wall layers [23].

2.3 Polymorphic crystalline structure in cellulose

Cellulose is a polymorph that can assume different crystalline structures. The two most common types of polymorphs are cellulose I and II, which are native and regenerated cellulose, respectively. The naturally found cellulose I exist in two types,

cellulose Iα and Iβ [33, 34]. Cellulose Iα with a triclinic crystalline structure is mostly produced by algae and bacteria, while cellulose Iβ with a monoclinic crystalline structure is mostly produced by terrestrial plants [35, 36].

The hydrogen bonds between the glucose monomer units play a crucial role in the cellulose structure. Hydrogen bonds are formed between hydroxy groups of inter- and intrachain residues. Intrachain hydrogen bonds exist between (O3-H---O5) and (O2-H---O6) groups [37, 38]. Adjacent cellulose chains are linked together by (O6-H---O3) hydrogen bonds that form a sheet-like structure [39, 40]. Additional interactions, such as ionic interaction and van der Waal's interactions, are needed to create crystalline orders. For example, the planar structures in the nanofibrils are held together by van der Waal's interactions and contribute to forming the crystalline structure [41].

2.4 Cellulosic fines

Fines are particles of a fibre suspension that can pass through holes of a certain size. Official standards suggest separating fines from the long-fibre fraction with a metal plate with round holes of 76 μm diametre or with a 200-mesh screen [42, 43]. The fines fraction can include short fibres, fibre wall fragments, and cells of other types depending on the kind of pulp [44, 45]. The two factors that distinguish fines from dissolved or colloidal dispersed materials, which can also pass through the screen, are: one, that fines are particles (i.e. retained on a filter paper [43]), and that they are visible in a light microscope [46].

There are two types of fines: primary fines and secondary fines (see Figure 4). Primary fines are those that arise during the original pulping process, i.e., mild mechanical treatment, and appear to be mostly flake-like with rectangular fragments of ray parenchyma cells. Secondary fines are created during additional treatment of the fibres, such as during mechanical beating, and appear more fibrillar-like in morphology [44, 47]. Chemical modification can also generate fines depending on

the intensity of modification of the fibre wall, which is discussed further in Chapter 4.

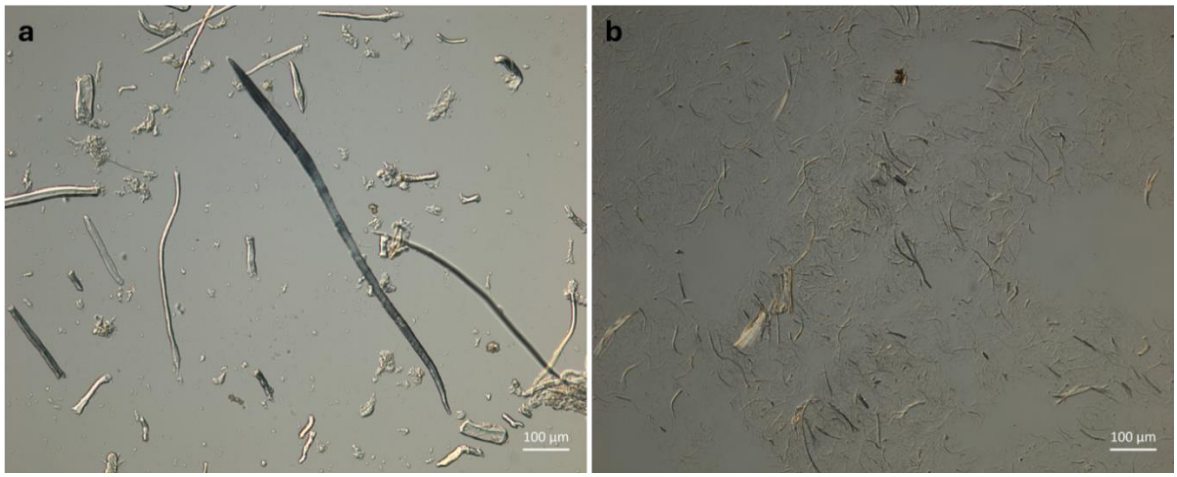

Figure 4. Images of (a) primary fines, the flake-like fragments of fibres and fragments of fibres, and (b) secondary fines which are mostly fibrillar material.

The mechanical properties of sheets of paper are affected by the presence of fines, in which fines densify the fibre network [47, 48], thereby increasing the number of inter-fibre bonds and the area in contact, which are the main factors affecting sheet strength besides the strength of the individual fibres [49]. Both primary and secondary fines improve the strength properties of paper. However, the effects are more pronounced for secondary fines [50], which may be due to structural differences. Depending on the nature of the fines, the relationship between the presence of fines and the different strength properties of hand sheets or paper mainly relies on the fines-fibre mixing ratio.

2.5 Dialcohol cellulose (DALC) fibres

To make dialcohol cellulose, cellulose is chemically modified by a two-step modification of periodate oxidation followed by borohydride reduction. The periodate oxidation, using sodium (meta) periodate ($NaIO_4$), is a selective oxidation that cleaves the bond between two vicinal functional groups, such as 1,2-diols, 1,2-amino alcohols, 1,2-hydroxy aldehydes, 1,2-ketones, and 1,2-amino aldehydes. In cellulose and some polysaccharides, the periodate effectively cleaves the C2-C3 bond

and forms a dialdehydes [51-55]. The partial chemical modification of solid cellulose DALC is a heterogenous chemical modification, in which it has been suggested that the DALC surrounds the crystalline core of cellulose, creating a core-shell model structure at the nanofibril level [7]. However, an extensive reaction leading to a higher degree of modification can reduce the crystalline regions of the cellulose nanocrystals [56-58]. In some studies, the reactivity of the periodate oxidation of cellulose is reported to be improved by ultrasound treatment [59], pulp size reduction before oxidation [60], a high-temperature reaction, or the addition of salts [61]. The aldehydes formed after periodate oxidation are further reduced to DALC by sodium borohydride. During the reduction of dialdehyde cellulose, it has been suggested that the depolymerisation of cellulose can be eliminated by controlling the alkalinity [62].

2.6 Structure of cellulose using x-ray scattering techniques

X-ray scattering techniques, such as small-angle x-ray scattering (SAXS) and wide-angle x-ray scattering (WAXS), were used to characterise the cellulose and DALC fibres of different DOMs at nanometre and Angstrom scales. The degree of cellulose crystallinity for DOMs in DALC has previously been studied using WAXS [6, 8, 63-65]. In this thesis, we adopted this 18-chain model only for the purpose of illustrating different planes. The cellulose unit cell with different planes, (200) in pink, (1-10) in blue, and (110) in orange, were considered parallel to the chain, and the (004) plane shown in black was perpendicular to the chain, as shown in the schematic below (Figure 5).

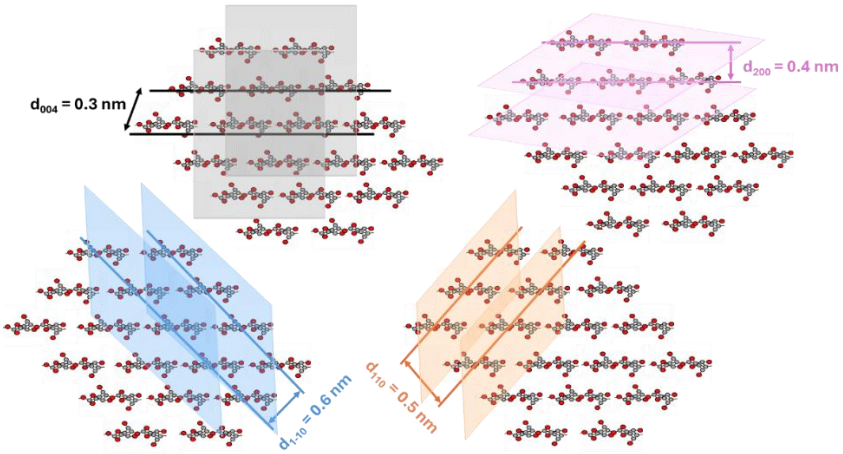

Figure 5. The different scattering planes of the cellulose nanofibrils [66].

The SAXS technique is suggested to show a peak corresponding to distance "d", between the nanofibrils or bundles of nanofibrils [67]. Pentillä et al. (2019) observed that the d-spacing changed between the dry and wet states, and as well as for different types of wood [67]. The SAXS curves have the shape of a shoulder in the scattering vector q, that appear between 0.1 and 0.3 $Å^{-1}$, carrying information on the lateral packing of the cellulose nanofibrils and nanofibril bundles [67, 68] (see Figure 2). Note that in the literature, these shoulders, which are transferred to clear peaks in the Kratky plots have been referred to by different names, such as SAXS data with q ranges [16] or inflection points [69]. In this thesis, we refer to the shoulder as the SAXS peak. Such wet and dry cellulose nanofibril structures have been extensively investigated and modelled in recent years [16, 20]. It is important to remember that the aggregation of these nanofibril bundles may vary along the length of the fibre, and SAXS measurements only provide the average distance and not the distribution of distances. There is still a discussion around the meaning of d-spacing in these SAXS measurements, where it can be: (i) the distance between the nanofibrils or the bundle of nanofibrils [20], or (ii) or size of the bundle of nanofibrils [16], or it cannot be theoretically excluded that it might also correspond to the size of the nanofibrils.

2.7 Morphology of cellulose fibres using microscopy techniques

The morphology and structures of cellulose fibres can influence the properties of the final material. Therefore, a better understanding of the morphology of natural or modified fibres is necessary for developing cellulose-based products. In this thesis, optical microscopies (OM): polarisation microscopy (PM), Differential interference contrast (DIC), and confocal laser scanning microscopy (CLSM) techniques have been used to elucidate the morphology of cellulose and DALC fibres at different DOMs.

2.7.1 Polarisation microscopy

Birefringence is the double refraction of light in a transparent and molecularly ordered material, which is manifested by the existence of orientation-dependent differences in refractive index in an optically anisotropic material. To create a birefringent image, the microscope must be equipped with both a polariser, positioned in the light path before the specimen, and an analyser (a second polariser, see Figure 6a), placed in the optical pathway between the objective lens and the eyepiece. The refracted and split light is then recombined using constructive and destructive interference by the analyser. This leads to the final generation of a high-contrast image.

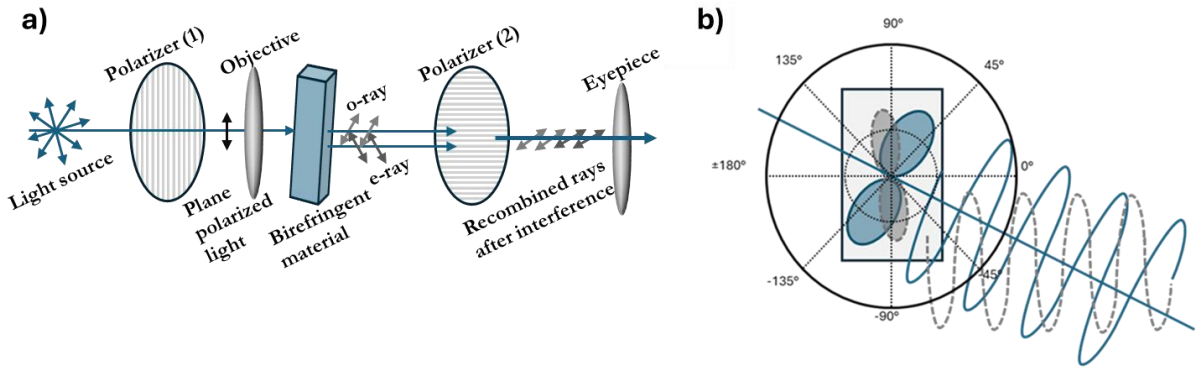

Figure 6. a) Schematic image of the setup of a polarised microscope; **b)** Schematic of birefringent of polarised microscopy created from the elliptically polarised light.

2.7.2 Differential interference contrast microscopy

DIC microscopy uses polarised light to convert phase delays into intensity changes (contrast). The effect is called "differential" because the contrast is created only in neighboring areas (e.g., at the interface of the fibre and the water in which it is suspended) because structures with different refractive indices are contrasted when in close contact with each other. The images produced using DIC microscopy are called pseudo-3D images of the specimen because the 2D images created appear as if they are illuminated from the side, while the opposite side remains dark. However, there is no light coming from sideways, the specimen is always illuminated by the light source. The light from the source is polarised by the polariser placed at an angle of 45° and the analyzer is placed at 135°. The important component of the DIC setup is a Nomarski prism. A Nomarski prism splits the polarised light ray in the DIC setup into two parts: the e-rays and the o-rays with electric field vectors oriented 90° with respect to each other. When polarised light travels through the Nomarski prism (1), the light splits into e-rays and o-rays, travels through the specimen and then encounters the Nomarski prism (2). The second Nomarski prism combines the e-rays and o-rays into a single ray, which then passes through the analyser and finally through the eyepiece, as shown in Figure. 7a. The image that is obtained looks like a 3D image (see Figure. 7b).

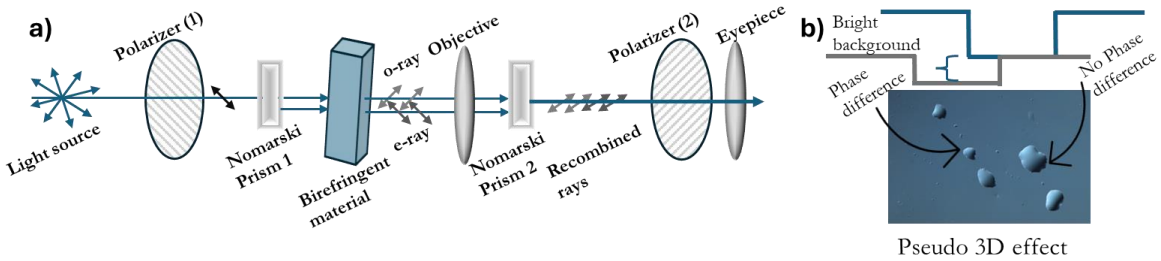

Figure 7. a) Schematics of DIC microscopy setup; **b)** Pseudo-3D images of DIC microscopy.

2.7.3 Confocal laser scanning microscopy

Light microscopy passes the light from the light source through the sample as uniformly as possible over the field of view. In the case of thicker samples, the objective lens does not have sufficient focus depth. The out-of-focus light will make the image more blurry, reducing the resolution. In ordinary fluorescence microscopy, any dye molecules in the field of view will be excited, including those in out-of-focus planes. In contrast, in confocal microscopy, only the dye molecules in the focal plane will be excited, and a pinhole inside the optical pathway will reject light that is out-of-focus to decrease the blur in the images.

The principle of confocal optics is as follows. A light beam from a laser source is reflected by a dichroic mirror, passes through a lens (objective) and focuses on the specimen. The chromophore in the specimen absorbs and emits light with a higher wavelength than the excitation wavelength. The emitted light passes through the same lens again but in the opposite direction. Because the emitted wavelength is larger than the excitation beam, the emitted light is not reflected in the dichroic mirror. Instead, it passes through the dichroic mirror and enters the photodetector. Confocal microscopy has two focal points, one at the sample and the other at the photodetector. Only the beams that are focused on the specimen form a second focus at the photodetector and reach the detector (see Figure 8). This technique allows for high-resolution imaging of thick specimens. Furthermore, by stacking several images from different optical planes using a suitable microscopy deconvolution software (z-stack), 3D structures can be analysed. It is also possible to analyse multicolour fluorescence staining using several lasers and emission/excitation filters.

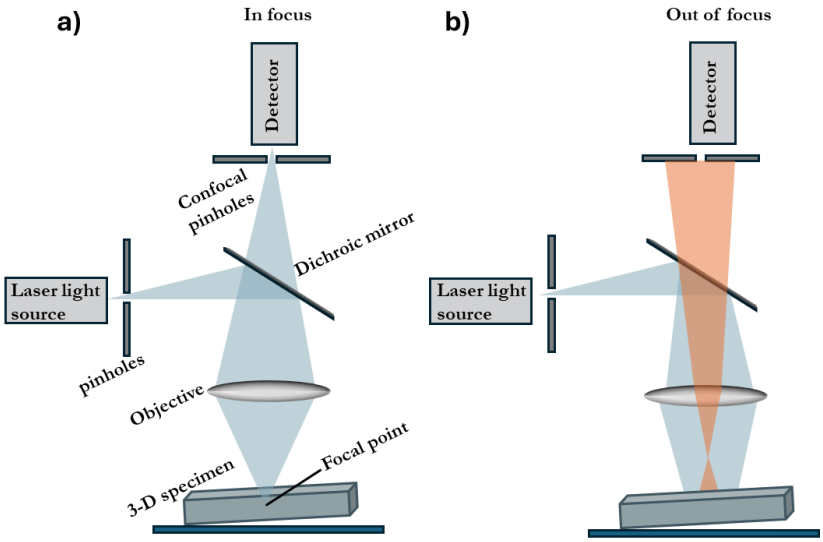

Figure 8. Schematic images showing a) in-focus and b) out-of-focus imaging in CLSM.

3. Materials and methods

3.1 Materials – preparation of dialcohol cellulose

3.1.1 Materials

Bleached softwood kraft fibres were supplied by Stora Enso and were mechanically beaten in a Voith mill at 160 kW h/tonne. Fines were removed by filtration. Sodium (meta)periodate was purchased from Sisco Research Laboratories, (99%) and 2-propanol from Supelco® (≥99.5%,). Sodium borohydride pellets were purchased from Thermo Scientific (98%). Filter bags of analytical grade (size 2, BPENG 200 μm) were purchased from a Filter Specialists Incorporated (FSI) filter. Other chemicals, such as sodium hydroxide, isopropanol, monobasic sodium phosphate, and hydroxylamine hydrochloride, were all analytical grades.

3.1.2 Preparation of dialcohol cellulose fibres

Bleached kraft fibres were chemically modified, first by oxidation with sodium (meta)periodate followed by reduction with sodium borohydride, partially converting the glucose units in the cellulose to ring-opened units. The cellulose sample, 39 kg of suspended pulp (4.5 wt% in deionized water), was heated to 44–50 °C in a 50 L mechanically stirred reactor (Hastelloy, UNS N06022) at RISE Processum (Örnsköldsvik, Sweden). Upon reaching the set temperature, 2.5 L of 2-propanol and 2.5 kg of sodium periodate were added. After oxidation for 45, 80, or 120 min, the reaction was stopped by thoroughly washing the samples in the filter bags with deionized water.

The oxidation step was followed by converting the aldehydes into primary alcohols, by resuspending the fibres in the 50 L mechanically stirred reactor. A total weight of 29.5 kg of the pulp suspension and 7.5 kg of ice were added. When the

temperature dropped below 4 °C, 350 g of sodium borohydride dissolved in 1.65 kg of deionized water was added for 3 min. After 1 h, the modified fibres were thoroughly washed with deionized water in filter bags to stop the reaction. After the oxidation and reduction modifications, the total gravimetric yields were 70, 40, and 30% for never-dried (ND) 26DOM, 44DOM, and 51DOM, respectively.

Specific amounts of the modified ND fibres were bench-dried (BD) at ambient temperature for 2–3 days. For rewet (RW) samples, 90% water was added and left to equilibrate for one day before any measurement.

The amount of aldehydes introduced in the oxidized cellulose was determined by stoichiometric reaction with hydroxylamine hydrochloride [70]. The amount of aldehyde concentration in the 26DOM, 44DOM, and 51DOM fibres was 3.1, 5.0, and 5.8 mmol g^{-1} of fibre, respectively.

The DOM was also measured using DNP-enhanced solid-state NMR spectroscopy, using the methods described by Karlsson et al. [71]. NMR experiments were performed on a Bruker 400 MHz DNP-spectrometer equipped with a 263 GHz gyrotron as a microwave source. DALC fibre samples were wetted/swelled in 12 mM AMUPol radical solution, consisting of DMSO:D_2O:H_2O in volumetric proportions of 6:3:1. 13C Multiple-contact cross-polarisation experiments were then performed with eight repetitions of the cross-polarisation step. The DOM was calculated from the increase in signal in the 56.4-69.4 ppm region.

3.2 Methods of characterisation

3.2.1 Fibre size analysis

3.2.1.1 Gravimetric determination of fines

The amount of "fines" in unmodified fibres and modified DALC fibres with three different DOM was determined using a Britt dynamic drainage jar (BDDJ) equipped with a screen with 76 μm diameter circular holes (Paper Research Materials, Seattle WA, USA). The starting materials (0.5 g initial dry mass) were suspended in 1.5 L of water. The fines were removed by continuous stirring (800 rpm). The impeller was adjusted to direct the pressure towards the screen, causing a flow that effectively prevented the sedimentation of fibres during the screening (see Figure 9).

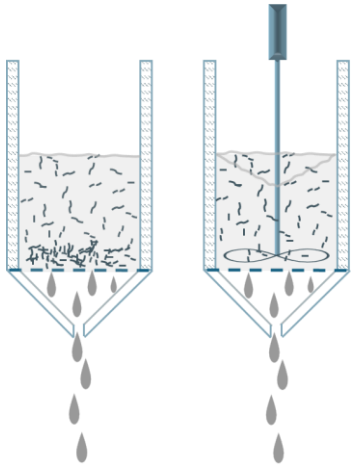

Figure 9. Illustration of fibre suspension when an impeller is used for gentle stirring during filtration.

After the screening, the fibres fraction (retentate) was separated from the fines fraction (filtrate). The obtained fibre fractions were oven-dried and weighed using pre-weighed filter papers. Because vacuum filtration of fines is tedious, the mass of fines was calculated as the original mass of the sample minus the mass of the retentate. Henceforth, this study will call these fine fractions "filtrates". This filtrate contains fragments of fibres, dispersed nanofibrils, and soluble components of DALC. Figure 4 shows some of the fragments of fibres from the filtrate images

under an optical microscope. All the prepared modified fibre samples and the control unmodified fibre samples were measured twice with two sample sets. The retentate for different DOMs was then bench-dried and labelled as BDXDOM-f where X denotes the DOM and "-f" denotes the fibre samples that was washed using the BDDJ process and then bench-dried.

3.2.1.2 Automated optical fibre analysis

A Kajaani FS300 (Metso Automation, Finland) was used to assess fibre properties such as numerical average fibre length, width, and kinks, etc. (according to Tappi T271). The instrument was calibrated before use by running a sample of synthetic (rayon) calibration fibres. Fibre length determinations were achieved with the optics system with a polariser adjusted to the 0–7.0 mm measuring range. Metso Automation software at Kajaani measured never-dried fibre samples by using the Kajaani Fibre Lab from screened pulps.

3.2.2 Analysis of water content in the fibres

3.2.2.1 Water retention value – quantitative

A mini water retention value method (WRV) method was used to determine the fibre swelling propensity gravimetrically, using a standard condition of centrifugal force of 3000 ± 50g (g is gravitational acceleration). A UFC40SV25 Ultrafree®-CL Centrifugal Filter of size from Sigma-Aldrich was used. A test pad of fibre with a dry mass of 0.05 g was centrifuged for 30 min.

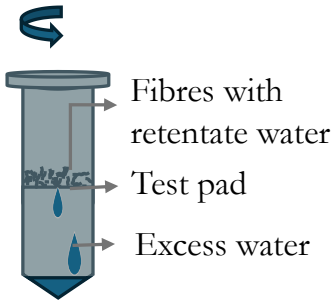

Figure 10. Illustration of the fibre after centrifugation on a test pad

These centrifuged test pads were weighed, oven-dried at 105 °C overnight, and then weighed again. The results are presented as g_{water}/g_{fibres} of dry fibres (see Figure. 10). The test pad was used with the centrifuge maintaining a working temperature of 23 ± 3 °C. The centrifuge was equipped with a timer and an electric brake. WRV is a simple and faster technique to estimate the swelling propensity of the fibre. To be able to measure the degree of swelling on the DALC fibres to improve the accuracy of swelling propensity, it is important to remove fines present in the modified fibre suspension in a BDDJ. All the prepared modified fibre samples and the control unmodified fibre samples were measured as duplicates.

3.2.2.2 Optical microscopy and image analysis - qualitative

Optical microscopy images were taken using a ZEISS Microscope (Oberkochen, Germany) in reflected light mode using cross-polarised light mode with an exposure time of 300–330 ms. In DIC mode an exposure time of 500 ms was used. To image wet and swollen fibres, a straightforward setup was employed using a glass slide (76 mm × 26 mm × 1 mm, VWR microscope slides, with cut edges frosted) and a cover slip (60 mm x 26 mm, Menzel-Gläzer, Charleston Scientific, Singapore), in which the edges of the coverslip were sealed using nail polish to avoid drying during imaging. All the imaging was done on the fibres suspended in excess water. ImageJ software (Maryland, USA) was used to manually measure the width of the water-swollen cellulose fibres.

3.2.2.3 Confocal laser scanning microscopy - qualitative

A Leica SP2 confocal laser scanning microscope (Leica Microsystems GmbH, Wetzlar, Germany) equipped with a 20× water immersion objective (Numerical Aperture = 0.5) was used for imaging with either 1 or 2× electronic magnification, with the following settings:

DIC = 1920 × 1200 pixels format was applied, yielding a pixel size of 0.386μm/px,

Confocal = 512 × 512 pixels, yielding a pixel size of 1.239 μm/px, and an image acquisition rate of two images per second.

The pinhole size was kept at 1 Airy Unit with a zoom factor of 4 for all experiments. The laser was a 100 mW argon laser, operating at a power level of 25%. Calcofluor white and fluorescein isothiocyanate (FITC) dextran with a molecular weight of 10 kDa were used for fluorescence imaging. Excitation was performed at 350 nm and emission was collected at 432 nm for Calcofluor. For FITC dextran, excitation was performed at 490 nm, and emission was collected at 520 nm. The FITC-labelled dextran was added to the sample suspension and left to defuse overnight while calcofluor white was added right before imaging. Three representative videos for each fibre sample were taken for analysis.

3.2.2 X-ray scattering techniques

The x-ray scatting experiments were done using Mat: Nordic (SAXSLAB/Xenocs) with a continuously variable sample-to-detector distance. This made it possible to measure extended SAXS (ESAXS), SAXS, middle angle x-ray scattering (MAXS), WAXS, and extended WAXS (EWAXS) over a q-range 0.003-2.5 $Å^{-1}$.

The x-ray source: A Rigaku 003+ high brilliance microfocus Cu-K radiation source (1.5406 Å) was used with Pilatus 300K and Pilatus 100K WAXS detectors.

Sample-detector distances for the different techniques: The major difference between the ESAXS, SAXS, MAXS, and WAXS is the sample-to-detector distance. The samples were mounted at ~1534 mm, ~1084 mm, ~484 mm, and ~134 mm for ESAXS, SAXS, MAXS, and WAXS measurements, respectively. The sample-detector distance was further reduced <~25 mm for EWAXS measurement to achieve q

values of up to 3 $Å^{-1}$, covering where the water peak begins (from q = 2 $Å^{-1}$). This was accomplished by attaching a 3D-printed extender piece to the sample mount.

Beam sizes for the different techniques: The beam sizes were adjusted to a diametre of 0.2 mm, 0.3 mm, 0.4 mm, 0.9 mm, and >0.9 mm for ESAXS, SAXS, MAXS, WAXS, and EWAXS measurements, respectively. All measurements were performed at a sample temperature of 25 °C with a beam path pressure of 1–2 mbar.

Sample preparation: The instrument operates under a vacuum, in which samples are mounted in a hermetically sealed compartment. To be able to measure the scattering of wet fibres, sandwich cell holders with Kapton tape windows were used. The bench-dried samples were directly taped on the sample mount.

Beam time: The dried samples were exposed for 60 min in all the measurements to get a good signal-to-noise ratio, whereas the never-dried and rewetted samples were exposed to 90 min because they contained water, which absorbed significant amounts of x-rays. The bench-top scattering equipment did not cause any beam time exposure. The acceleration of photons was 24.6, 13.9, 2.0, and 1.0 m/s^2 for WAXS, MAXS, SAXS, and ESAXS, respectively. The background scattering of Kapton and water was also measured using the same exposure time as the samples. The water scattering was measured in a capillary tube filled with water.

The absolute intensity of the measured scattering pattern was estimated by comparison with the direct beam intensity for both SAXS and WAXS. Data reduction was done with SAXSGUI software (version 2.27.03). The thickness correction and subtraction of the backgrounds were done using the Origin software program. The data was visualized as SAXS curves showing intensity on the y-axis and q from0.002 $Å^{-1}$ to 0.7 $Å^{-1}$ on the x-axis. For WAXS curves, the y-axis was the intensity, and the x-axis was q from 0.3 $Å^{-1}$ to 3 $Å^{-1}$.

Data treatment: In both SAXS and WAXS the direct beam intensity was measured to determine the absolute intensity of the measured scattering pattern. Data reduction was done with SAXSGUI software (version 2.27.03). The thickness

correction and subtraction of the background (such as Kapton, and water) were done using the Origin software program. The background subtraction was carried out by subtracting the measured empty Kapton window. To subtract the water peaks from the scattered fibre curves, the scattering data of the empty capillary tube was first subtracted. This gave true water scattering data which was later subtracted from the sample data. All the prepared modified fibre samples and the control unmodified fibre samples were measured twice with two sample sets and the x-ray scattering results are the averages of the two measurement sets.

4. Results and Discussion

4.1 Assessment of fines and degree of modification for partially modified DALC

The results showed a similar degree of oxidation (DO) with the titration values as the NMR-determined DOM values (see Table 1). The titration method determined the number of aldehydes present in the sample after periodate oxidation, which later were reduced by sodium borohydride into alcohol groups. As the reduction step should only reduce the already oxidized regions of the glucose units in cellulose chains, the degree of oxidation was assumed to be the DOM as long as there were not any major losses of mass. The NMR measurement results for the sample with the filtrate and the DO from the titration appear to corroborate with each other.

The never-dried DALC fibres were filtered using a BDDJ to assess the weight fraction of filtrate that passed through the sieve (openings of 76 μm). The filtrate content for different samples is given in Table 1. As shown in Table 1, the dry mass of the filtrate for ND26DOM was less than 10%, while for ND44DOM and ND51DOM, it was ~30%. The ND44DOM and ND51DOM samples with the lowest yield gave the lowest retentate fraction. This filtered fraction could arise due to modification. The filtrate fraction for the modified DALC samples was not characterised but likely contained parts of smaller fibre fragments, including partially dispersed nanofibrils, and soluble components of DALC.

The DNP-NMR was further done on bench-dried retentate from the BDDJ. Table 1 shows that DNP-NMR determined DOM was lower for the samples when the filtrate was removed using the BDDJ, indicating that the filtrate had a higher DOM. The fact that the DOMs differ between the NMR values with and without filtrate suggests that there could be a predominant loss of modified material (as

filtrate) from the BDDJ washing, i.e., the removed material has a higher DOM. One reason the filtrate material was not washed away during the production step could be due to inefficient washing, or because the subsequent drying of ND to BD fibres, rewetting, and stirring of the fibres during the BDDJ fractionation damaged the fibres, facilitating the leaking out of materials. After the reduction step, the fibres were washed with high consistency which was enough to remove the chemicals, but maybe not sufficient to remove the fine materials.

The DOM of the solids in the filtrate was back calculated from the fractions sizes and the DOMs determined by NMR (of the starting material and the material without fines). The calculated DOM of the filtrate was larger for all the modified samples. This showed that the washed filtrate carried substantial amounts of modified material. The calculated value for 26DOM was >100%, which shows that there was some uncertainty in the measurements. The reason for the higher DOMs for the filtrates could be due to insufficient washing, i.e., removal of matter in the BDDJ.

Table 1. Filtrate content and the degree of modification of the fibres used in this study.

DOM	Filtrate (%)	DO using Titration (%)	DOM using NMR before BDDJ (%)	DOM using NMR after BDDJ (%)	Calculated DOM of filtrate (%)
ND0DOM	1.4*	NA	NA	NA	NA
ND26DOM	5.0 ± 1.3	26	24	18	138**
ND44DOM	33.7 ± 1.5	44	42	35	56
ND51DOM	26.7 ± 3.0	51	51	45	67

* Only one measurement was made for this sample. **This value is unrealistic because it is above 100%.

The filtrate % values are given with error, calculated as (max-min)/2.

All the benched dried samples, with and without fines (i.e., BDDJ treated and non-treated), were assessed for the DOM using DNP-enhanced solid-state NMR spectroscopy.

4.2 Swelling propensity of DALC with different degrees of modification at different length scales

4.2.1 Influence of modification on the structure of fibre at the nanoscale

4.2.1.1 WAXS studies of DALC fibres with different DOMs and sample treatments

The WAXS measurements were made on bench-dried samples of different DOMs before and after the BDDJ washing to compare the differences in the cellulose chains in the crystalline areas of the modified fibres, labelled "BDXDOM-f", where -f denotes the absence of fines. The increase in DOM decreases the scattering intensity for the bench-dried samples as shown in Figure 11, in which the WAXS curves plotted in dash lines are the retentate fibres showing higher scattering intensity due to lower DOM. The dotted lines in the graph corresponded to different planes in the fibres. Similar curves were shown in the literature, and it was interpreted that the higher the DALC modification was, the lesser was the ordering of the polymer chains [8, 63]. Furthermore, the WAXS data (Figure 11) indicated that the retentate samples exhibited higher peaks. These higher peaks for the samples after BDDJ washing (retentate) also corroborated with the lower DOM from the NMR measurements. The inter-planar spacings for the considered four crystallographic planes (1–10), (110), and (200) parallel to the chain, and (004) perpendicular to the chain, were the same for all DOMs and correspond to 0.6 nm, 0.5 nm, 0.4 nm, and 0.3 nm, respectively. This calculated inter-planar spacing was in accordance with a recent study by Hans *et al.* [66].

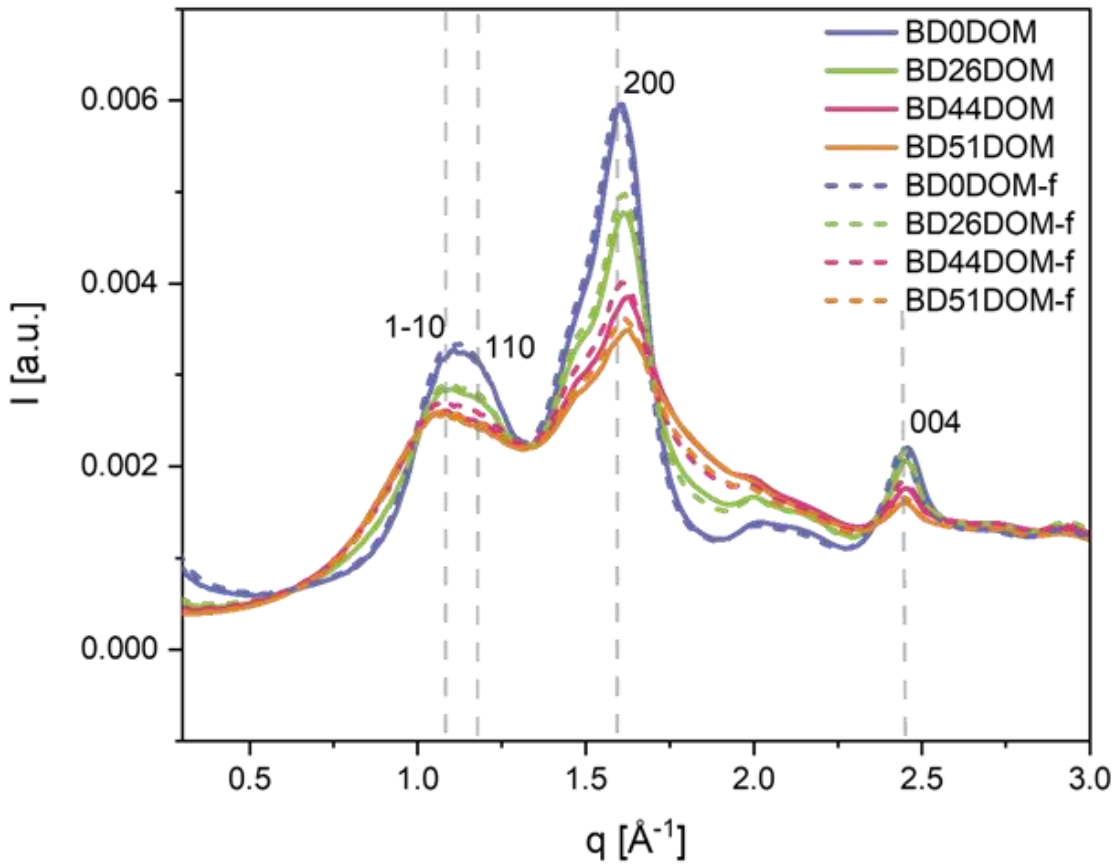

Figure 11. WAXS intensity as a function of q for the fibres of different DOM before and after washing. The dashed coloured lines are the washed fibres, while the solid coloured lines are the fibres containing fines and fragments before washing.

In Figure 12, it can be observed from the WAXS curve for the wet samples that for both the never-dried and rewetted samples, for the different DOM (at the same total mass of the dry sample) there was no shift in peaks observed in the wet samples, which indicated that the water did not destroy the core crystallinity of the cellulose. To further elucidate the fibre peaks, the water peaks were subtracted from the never-dried and rewetted fibre samples.

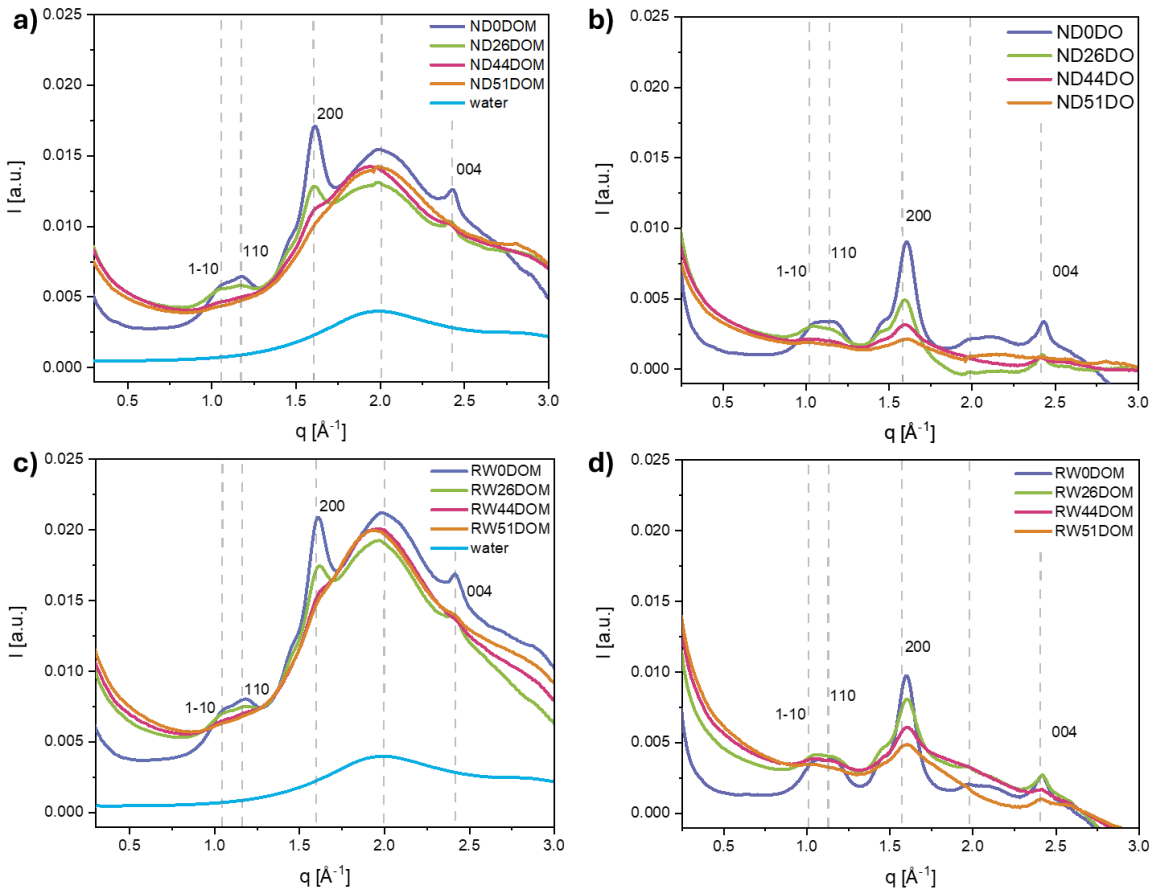

Figure 12. WAXS plot for a) the never-dried samples; b) the water-subtracted curves of never-dried samples, c) the rewetted samples, and; d) the water-subtracted curves of the rewetted samples.

4.2.1.2 SAXS studies of DALC fibres with different DOM

SAXS measurements were done on fibres with different DOMs with different conditions (never-dried, bench-dried, and rewetted) to compare the difference in the nano-swelling of the nanofibril bundles. As shown in Figure 13, for all the sample conditions (never-dried, bench-dried, and rewetted) the SAXS peaks became broader and moved towards the lower q values as the DOM increased. This could be interpreted as an increase in the distances between the nanofibrils and the nanofibril bundles with increasing DOMs, or as an increase in dimensions of the nanofibrils and nanofibril bundles with increasing DOMs. Both options would lead to swelling at the nano-level, hereafter referred to as "nano-swelling". The intensity

in SAXS curves for the wet samples, never-dried and rewetted, at q = 0.05, is about 40 times larger than the bench-dried curves in Figure 13. According to Penttilä et al. (2021), "the increased scattering observed in dry fibres is due to SAXS detecting a signal primarily from crystalline cellulose microfibrils embedded within a continuous water matrix, along with contributions from less-ordered polysaccharides and lignin. When the sample dries, the contrast conditions alter, making scattering from the surfaces of air-filled pores more pronounced, especially at lower scattering angles" [72]. However, the observations of increased scattering intensities at the SAXS peak for the wet fibres compared to dry fibres are still not clear.

Furthermore, the SAXS curves from the lower q region can be correlated to the power-law exponents which are dependent on the physical characteristics of the sample [73]. The slopes were less steep for never-dried and rewetted samples than the bench-dried ones. Furthermore, the slope decreased with increasing DOM for all the sample conditions. Such a change in the slope may indicate the change from dense aggregates of the swollen chains to a low-density, loosely packed aggregate of rod-like structures[74-76].

The swelling of nanofibril bundles or nanofibrils or the distance between the nanofibril bundles or nanofibrils for different DOMs for the never-dried, bench-dried, and rewetted conditions is often better estimated using Kratky plots (i.e., Iq^2 as a function of q). The nano-swelling for different DOMs of cellulose into DALC for the never-dried, bench-dried, and rewetted conditions was estimated using the Kratky plot shown in Table 2. The graphs of the estimated "nano-swelling" and the Kratky plots are given in the Supplementary Information of Manuscript 1. The SAXS peaks varied for bench-dried fibres from ~5 nm for BD0DOM to 11 nm for BD51DOM and never-dried fibres, it varied from ~11 nm for ND0DOM to ~21 nm for ND51DOM. For never-dried and rewetted samples fibres, i.e. wet fibres, the region in between the nanofibril bundles may have the possibility to accommodate water as the surface polymers from the nanofibrils are more loosely attached and hydrated, thereby causing an increase in the average nano-swelling from ~11 nm for

the ND0DOM to 14 nm, 17 nm, and 21 nm, for the ND26DOM, ND44DOM and ND51DOM, respectively.

Additionally, the observed decrease in the nano-swelling between the corresponding never-dried and rewetted samples could be due to hornification of nanofibrils and nanofibril bundles inside the fibre wall. Instrumental error bars (dI) are also plotted here by the 70% transparency markers in the same colour for all the curves.

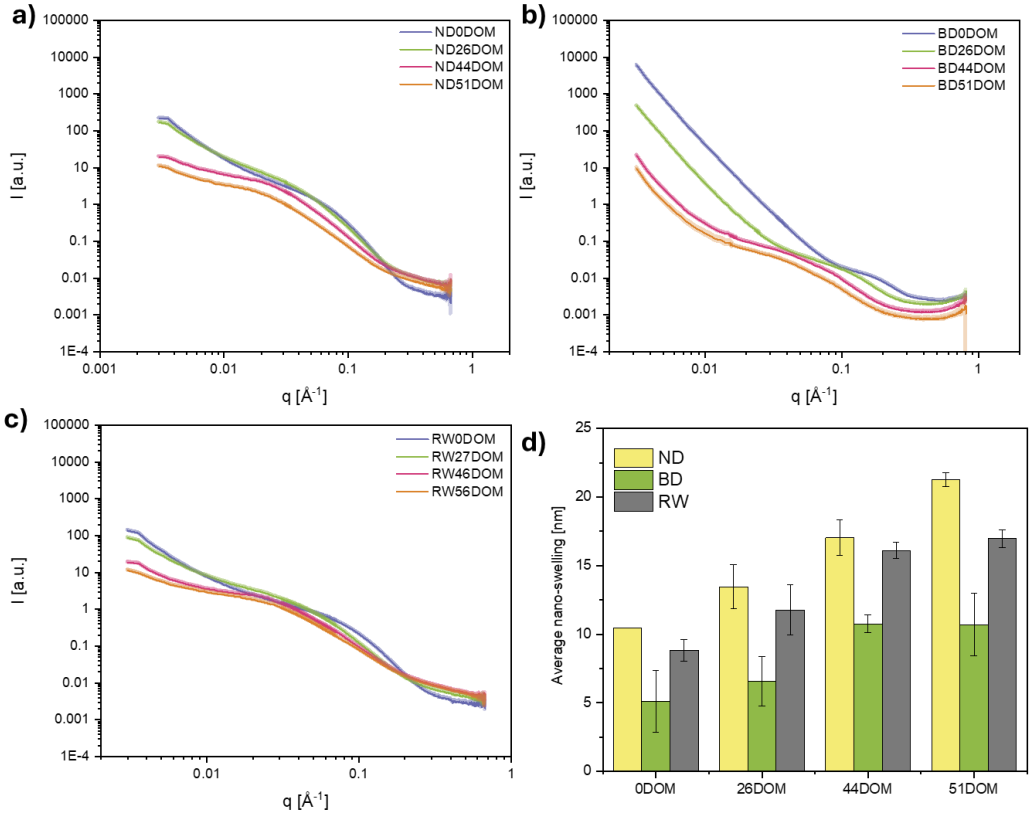

Figure 13. SAXS curves showing the scattering intensity vs q for a) ND samples, b) BD samples, and c) RW samples. Error bars for the experimental intensity are plotted. In most cases, error bars are covered by the markers. (d) Bar plot showing the average nano-swelling for ND, BD and RW samples for 0DOM, 26DOM, 44DOM and 51DOM. The measurements were made twice with two sample sets and the mean distance values are given with the error, calculated as (max-min)/2, obtained from two independent measurements.

Table 2. The nano-swelling for different degrees of modification of cellulose into dialcohol cellulose for the never-dried, bench-dried, and rewetted conditions was estimated using the Kratky plot.

Sample	ND0DOM		ND26DOM		ND44DOM		ND51DOM	
Peak centre in Kratky plot	0.060	0.060	0.043	0.051	0.035	0.039	0.029	0.030
d = 2π/q (nm)	10.5	10.5	14.6	12.3	17.9	16.1	21.7	20.9
average	10.5 (0.00)		13.5 (1.1)		17.0 (0.9)		21.3 (0.4)	
Sample	BD0DOM		BD26DOM		BD44DOM		BD51DOM	
Peak centre in Kratky plot	0.179	0.094	0.119	0.08	0.056	0.061	0.051	0.069
d = 2π/q (nm)	3.5	6.7	5.3	7.8	11.2	10.3	12.3	9.1
average	5.1 (1.6)		6.6 (1.3)		10.7 (0.5)		10.7 (1.6)	
Sample	RW0DOM		RW26DOM		RW44DOM		RW51DOM	
Peak centre in Kratky plot	0.075	0.067	0.048	0.060	0.039	0.038	0.038	0.036
d = 2π/q (nm)	8.4	9.4	13.1	10.5	16.1	16.5	16.5	17.4
average	8.8 (0.5)		11.8 (1.3)		16.3 (0.2)		17.0 (0.5)	

*The measurements were made twice with two sample sets and the mean distance values are given with error, calculated as (max-min)/2.

4.2.2 Swelling propensity at the microscale for different degrees of modification

4.2.2.1 Water retention value for the different DALC samples

The water retention value (WRV) was used to quantify the ability of the modified cellulose samples to hold water in the fibre network and in the single fibre. The measurements were made after the removal of fines from the samples. The WRV value for the ND0DOM and ND26DOM fibres were measured to be 1.7 and 3.4 g_{water}/g_{fibre}, respectively, which were close to the value obtained by Sjöstedt *et al.* of ~3.5 g/g for 24% DALC fibres [51]. The WRV increased with increasing DOM (Figure 14); for the higher DOM of 44 and 51%, the WRV increased to 4.9 g_{water}/g_{fibre} and 6.3 g_{water}/g_{fibre}, respectively.

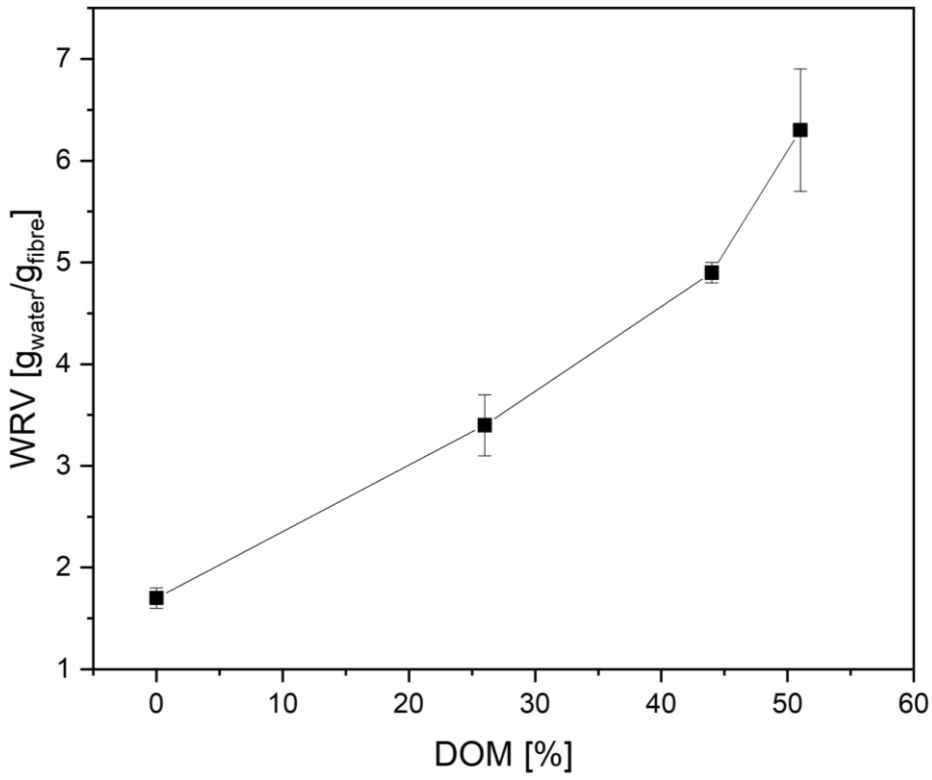

Figure 14. WRV as a function of the degree of modification (DOM) of the dialcohol cellulose (DALC) fibres.

The WRV depends on, for example, the type of fibre, fibre size, mechanical properties, and the presence of fragments of fibres or dissolved materials [77], commonly referred to as fines. This may indicate that the swelling propensity of the modified fibres increases with increasing DOM.

4.2.2.2 Optical Microscopy

Light microscopy was used to image the never-dried fibres to understand the morphological changes in the modified fibres and compare them with the unmodified fibre. DIC and polarisation modes of microscopy were used to complement each other for a better understanding of fibre morphology. The advantage of the DIC mode is that it gives a pseudo-3D effect of the fibres from the 2D microscopy images. Hence, it is possible to perceive more easily the

morphological changes of fibre, such as swelling, fibre damage, external fibre fibrillation, and orientation of different regions of the fibre wall. In comparison, the polarisation mode, on the other hand, is sensitive only to optically anisotropic fibre structures, indicating fibre ordering and the orientation of nanofibrils.

Figure 15 shows the comparison of fibre morphology observed by DIC and polarisation mode imaging. The images in the first column and the second column are all DIC and polarised images, respectively, in the same field of view. The top row images show ND0DOM fibres, exhibiting some kinks and curls (Figures 15a, and b). The ND26DOM images display a mild periodic bulging, but not full-scale ballooning, along the fibres (Figures 15c, and d). The tendency of a significant heterogeneously swollen fibre wall is more pronounced for ND44DOM, in which ballooning is readily visible, with the characteristic balloon-collar-like structures (Figure 15e, and f). The ND51DOM images appear to show the most extensive swelling and ballooning (Figure 15g, and h). It can also be seen that the cellulosic material within the balloons of the modified fibres became more transparent. This is presumably due to the dramatic swelling of the fibre, which causes minimal differences in refractive indices between the inside and outside environment of the balloons [78].

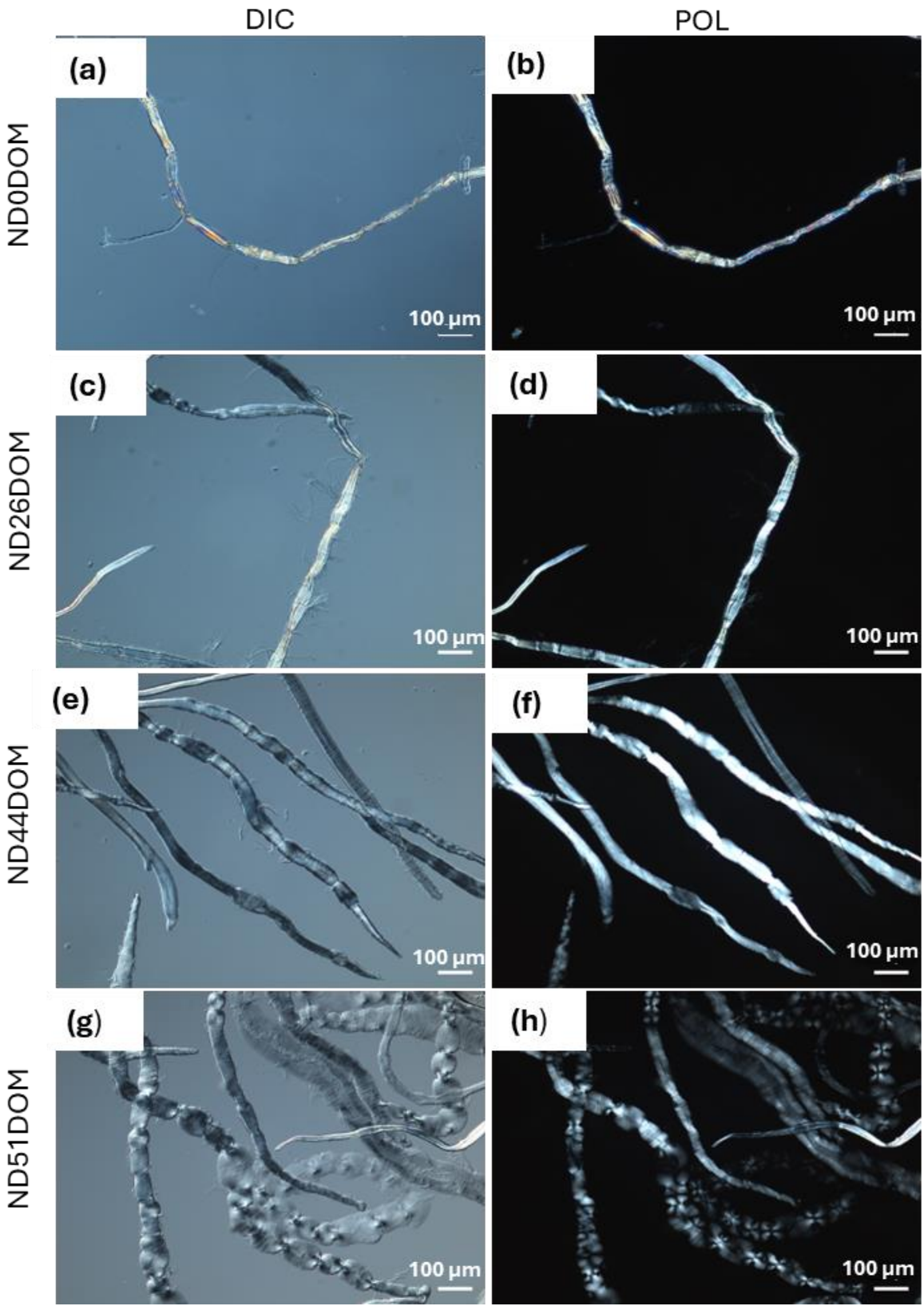

Figure 15. The same field of view was imaged with two different modes: DIC and polarisation. (a), (b) ND0DOM; (c), (d) ND26DOM; (e), (f) ND44DOM; (g), (h) ND51DOM in DIC and polarisation mode, respectively. All the images are representative of fibre samples.

A closer observation of these swollen fibres indicates an evolution of balloon-collar swelling. The heterogeneous chemical modification leads to heterogeneous fibre swelling in two ways: one, the heterogeneity in swelling along the fibre length (causing balloon-collar structure), and two, the heterogeneity in swelling among different fibres in the same DOM sample.

Furthermore, a clear mild bulging along the fibre wall of the DALC fibres was observed in a substantial population of the ND26DOM fibres, which marks the beginning of the ballooning phenomenon. It was also observed that a substantial number of fibres with uniform swelling along the fibre length (homogenously swollen fibres) was present alongside the highly swollen ballon-collared fibres in the ND51DOM fibres. These substantial fibre populations with homogenous swelling can indicate that the lateral swelling with balloon-collar morphology would not continue infinitely by increasing DOM. This can be verified from the image shown in a recent work, with partially modified DALC fibres of 55% DOM from a similar source (softwood kraft fibre), predominantly being homogeneously swollen with a few balloons [79].

Figure 16a shows a DIC image of the balloon-collar ND51DOM fibre, which has been previously discussed in detail earlier. Figures 16b,c,d shows DIC images of the homogenously swollen fibres of ND51DOM. The mechanism behind homogenous swelling could be that the larger balloons expand at the collar region, resulting in swelling of the collar region, thus merging two nearby balloons into one. When this happens all along the fibre length, it results in a homogenously swollen fibre. Figure 16 b-d shows a homogenously swollen fibre. A helical winding in the middle of the fibres can be observed. Additionally, Figure 16c,d shows a clear crumbling inside of the swollen fibre wall (marked in red circles). Such a helical winding in the middle of the swollen fibre was previously observed by Sim *et al.,* and was suggested to be the S3 layer [78]. Sim *et al.* have previously discussed in great detail the swelling of carboxymethylated and periodate–chlorite oxidized fibres, which results in a small

decrease in the fibre length. They suggest that this decrease induces a crumpling of the S3 layer, which generates a void between the S2 and S3 layers.

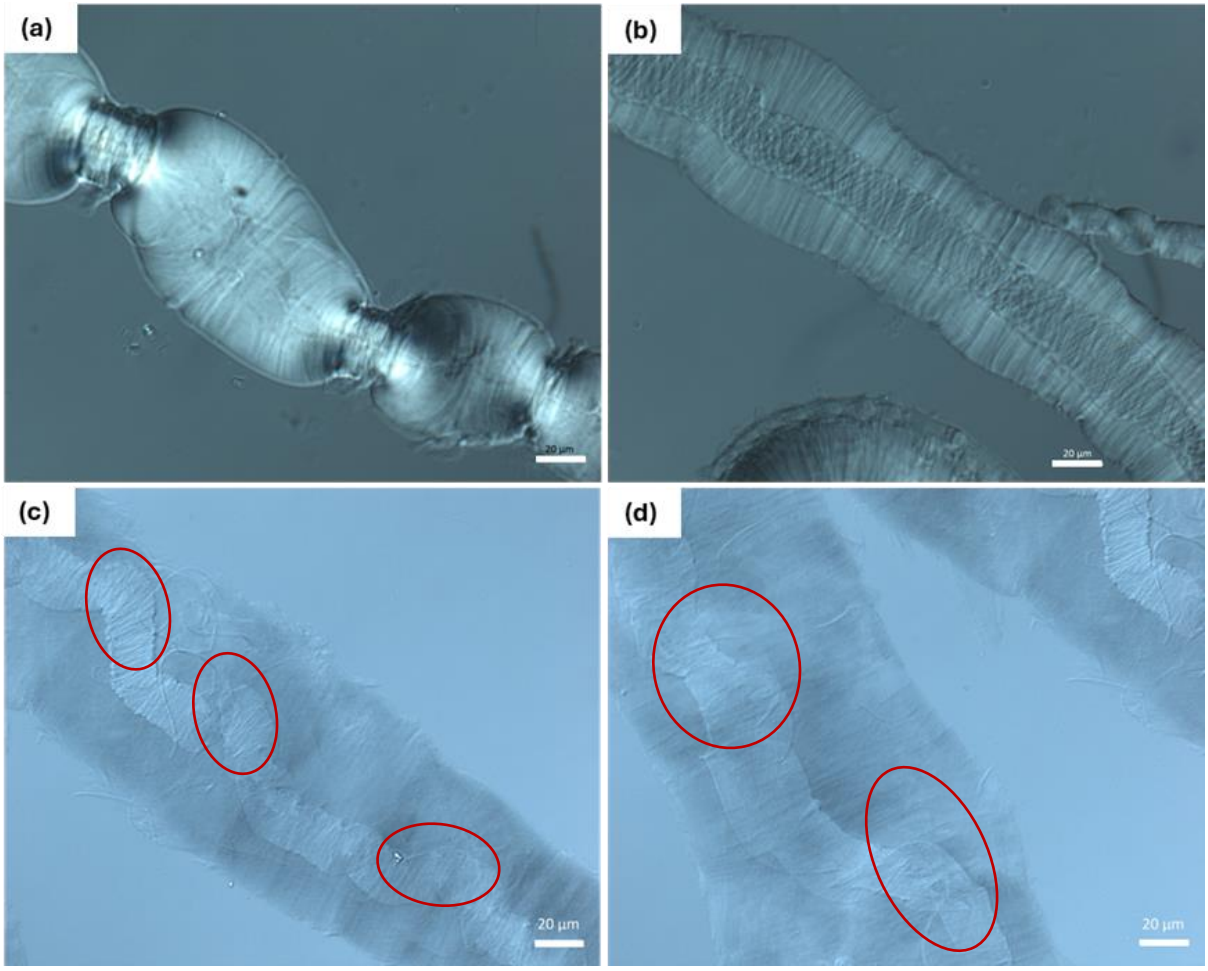

Figure 16. Swelling of ND51DOM fibres. (a) Heterogenous swelling. (b), (c), and (d) Homogenous swelling. All the fibres shown in the images are in DIC mode at 500× magnification. The crumbling inside the swollen fibre wall is marked in red circles. Scale bar = 20 µm.

When the fibres are immersed in water, the water can be retained in different locations, such as between the fibre network, in the lumen of fibres, and in the pores inside the fibre wall. When a native fibre swells, the fibre wall expands inwards, towards the lumen region [80]. However, the DALC fibres seem to swell differently. It is therefore of interest to understand the condition of the lumen region in these swollen DALC fibres. Using DIC and polarised images, it is not possible to visualise the lumen region inside the fibre wall. Hence, CLSM with fluorescent labelling was used, as it would be an ideal choice to understand these intricate details inside the

swollen fibre wall. The dual labelled fibres were imaged using CLSM along the z-direction through fibre width. The green colour in the images indicates the FITC dextran and the blue colour indicates the fibres. By this approach, it is possible to record the condition inside the fibre wall of these ballooned fibres.

Figure 17 shows the comparison of fibre morphology observed by DIC and CLSM imaging in the same field of view. The images in the first column are all DIC images and the second and third columns are all the CLSM images and CLSM of 3D z-scanned fibres of ND0DOM, ND26DOM, ND44DOM, and ND51DOM, respectively. In Figures 17b,c, the z-scanning through the ND0DOM fibre does not clearly show the FITC- dextran inside the lumen (lack of green colour). The presence of water is not quite evident in the lumen region of the swollen ND0DOM fibre. However, modification-induced ballooned fibres show a clear presence of FITC-dextran inside the lumen. Additionally, the presence of this phase increases with the increase in ballooning. This is evident in Figures 17e,h,k, in which a gradual increase in the FITC-dextran can be observed.

The ballooning scenario has been proposed and discussed in detail in previous works using a model that suggests the arrangements of the different secondary wall layers in the ballooned fibres [78], Our experimental results using dual-colour labelling in CLSM imaging have, for the first time revealed the expansion of the lumen region due to ballooning of the swollen fibres. By identifying the FITC-dextran at the center of the ballooned fibres, it is possible to indirectly show the expansion of the lumen. The expansion of the lumen can be caused by the substantial amount of nanofibrils from the S1 layer being rolled to make the collar region. As a result, there may not be enough of the S1 layer remaining across the balloons to resist the lateral swelling. This in turn may lead to the inner fibre wall layers (S2, and S3) being pushed outwards, enlarging the lumen.

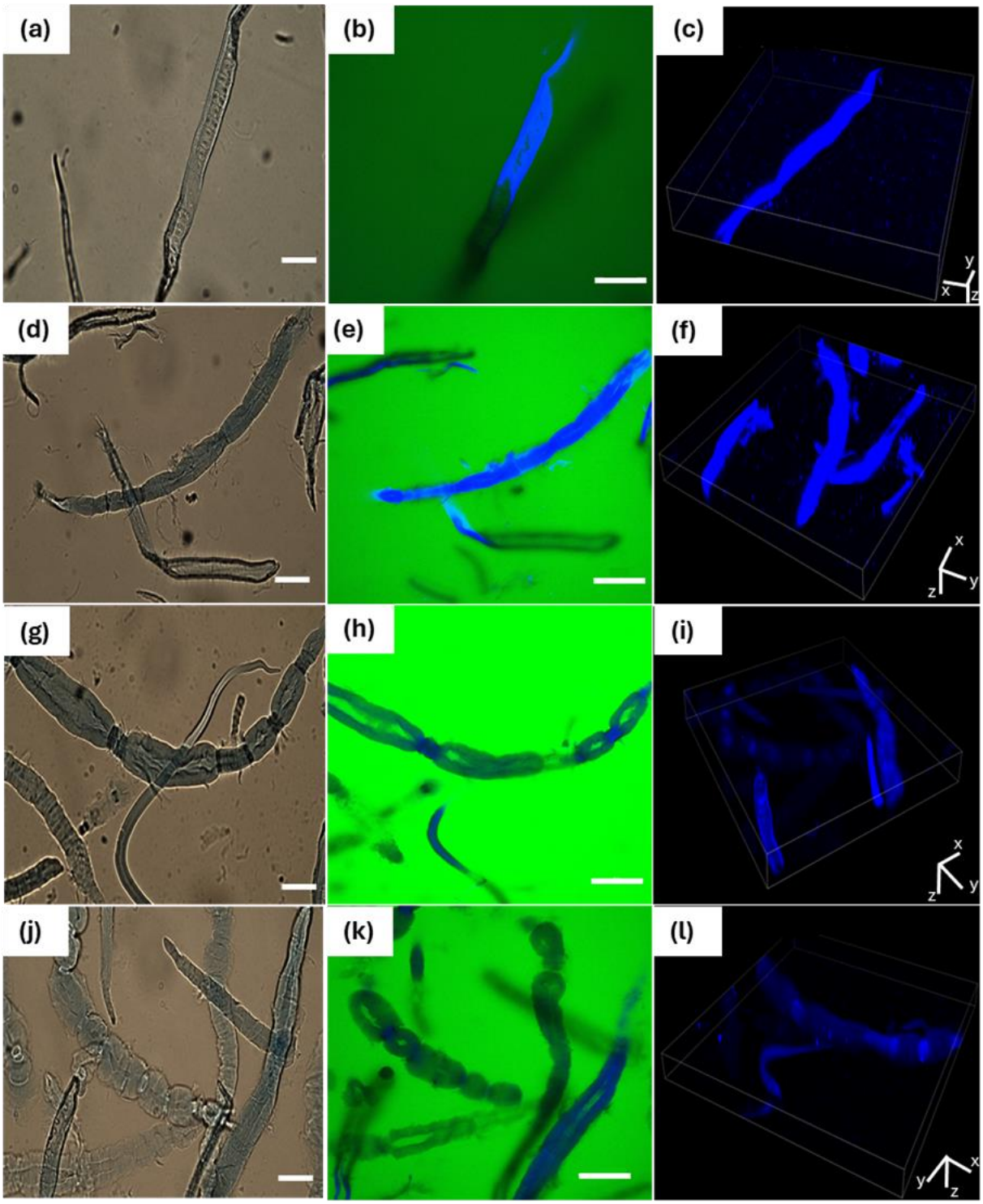

Figure 17. (a, d, g, j) DIC images of ND0DOM, ND26DOM, ND44DOM, and ND51DOM, respectively. (b, e, h, k) CLSM images of dual fluorescently labelled fibres of ND0DOM, ND26DOM, ND44DOM, and ND51DOM, respectively. Calcofluor - blue, FITC dextran - green. (c, f, i, l) CLSM of 3D z-scanned fibres of ND0DOM, ND26DOM, ND44DOM, and ND51DOM, respectively. All the images in each row are in the same field of view for easy comparison. Scale bar = 100 μm.

4.3 Correlation of swelling propensity between the nanometre scale and the micrometre scale.

The swelling propensities of the fibres were estimated using the WRV (explained in Section 4.2.2.1). It is a simple and indirect method that can be correlated to the swelling of fibres, assuming that no water has been retained by the networks and that the centrifugation has extracted pore water from the fibres. The swelling propensity of the fibres estimated from the WRV corroborates with the measured width of the swollen fibres from DIC images and the average nano-swelling values from the SAXS measurements. (see Figure 18a).

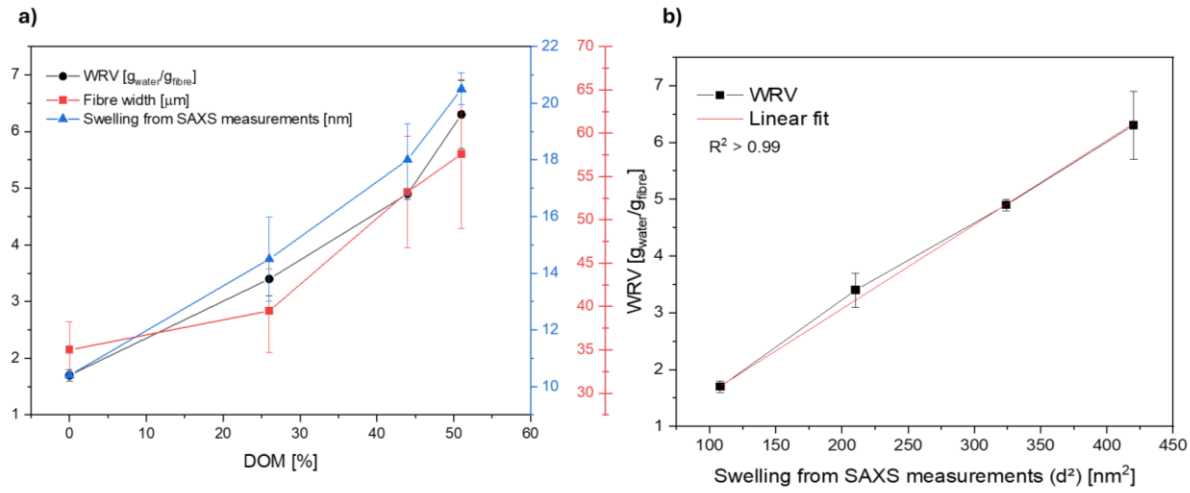

Figure 18. a) The change in WRV, measured fibre width, and the swelling from SAXS measurements as the DOM increases. b) The WRV versus swelling from SAXS measurements.

Interestingly, the swelling propensity of the fibre wall at the fibre level seems to have a linear correlation with the swelling observed from the SAXS measurements. This shows that the chemical modification of cellulose fibres to DALC fibres at the molecular level affects the morphology and structure at multiple length scales.

5. Conclusion

The overarching aim of this thesis has been to understand the swelling behaviour of partially modified DALC fibres with different DOMs and at different length scales, from nano to micro, using an assortment of characterisation techniques.

SAXS studies show that partial modification of never-dried DALC samples have nano-swelling with increasing DOM. Bench drying followed by rewetting of the fibres in water showed a similar increase in nano-swelling with increased DOM. This shows that the nanofibril bundles in the fibre wall are systematically loosened up by chemical modification, which can further enable the lignocellulosic material to be processed easily. Furthermore, a sign of hornification is observed from the decrease in nano-swelling of the never-dried and rewetted samples for the same DOM. The modification alters the core crystallinity of the cellulose, starting from the surface of the nanofibrils. This indicates an increased penetration of water in the disordered regions (shell region), which may be advantageous for material processing applications.

The microscopy studies provide a clear indication that when the softwood kraft fibres undergo partial heterogenous DALC modification, it may require ~25% DOM to observe a mild ballooning in a substantial population of the swollen fibres, and ~50% DOM constitutes a substantial amount of homogenously swollen fibres alongside the heterogeneous balloon-collar swelling. Using dual fluorescent labelling, the condition of the lumen in the ballooned fibres can be studied. Furthermore, bench drying followed by rewetting in deionised water showed a similar increase in swelling compared to the never-dried fibres with an increase in DOM. Interestingly, the swelling propensity as measured with the water retention values and the nano-swelling estimated from the SAXS peaks correlated linearly with each other ($R^2 > 0.99$), indicating that the SAXS peak correlates to the microscopic swelling of the fibre wall. Engel et al. (2025) recently demonstrated that DALC

fibres can be processed using water as a plasticizer, presenting a promising advancement for material processing applications [11]. This study may provide valuable insights into the mechanisms enabling water to function effectively as a plasticizer in this context.

6. Acknowledgments

This research was carried out within the industrial graduate school Resource-smart Processes, funded by the strategic innovation program BioInnovation - a joint venture of Vinnova, Formas, and the Energy Agency.

I would like to thank my supervisor Anette Larsson for her support, guidance, and brainstorming sessions. I would also like to thank my co-supervisor Per Larsson for aiding me with his competence in this endeavour.

I thank Tetra Pak for the industrial supervision of this project.

I thank my groups at BioInnvation and Resource Smart Processes and Vinnova Competence Centre FibRe for all their support and feedback on my work.

I also want to thank Dr Michal Strach from CMAL, Physics department, and Dr Shuichi Haraguchi, Chemistry, Chalmers, for their valuable guidance in the laboratory and most importantly Department of Chemistry for all their support.

I would like to thank my collaborators and co-authors for their contributions and interesting discussions.

I thank all my colleagues, friends and extended family with whom I have and will continue to create memories.

I would like to thank Dr Sriram KK, my best friend/husband/father of my son/ badminton mate/my personal nutritionist/ Research scientist at Life Science Department, Chalmers for his constant moral support throughout my journey.

Last but never least, I thank my child for making me a mom and being very protective of me day in and day out. At this point in our lives, I am not sure if I have taught you enough about understanding the world or if you have taught me more. I guess the latter is true as I am still learning more from you every day. This research work of mine would not have happened without your support. Love you, Ashwath.

7. References

1. Zeenat, et al., *Plastics degradation by microbes: A sustainable approach.* Journal of King Saud University - Science, 2021. **33**(6): p. 101538.
2. Ngo, H. *How do you fix healthcare's medical waste problem?* BBC Future 2020 [cited August 14, 2020]; Available from: https://www.bbc.com/future/article/20200813-the-hidden-harm-of-medical-plastic-waste-and-pollution.
3. *Plastics – the fast Facts, 2023*. 2023.
4. *Forest statistics 2020*. 2020.
5. Department, C., *Statistisk årsbok för Sverige, Statistical Year book of Sweden* 2011: Sweden.
6. Larsson, P.A., L.A. Berglund, and L. Wågberg, *Highly ductile fibres and sheets by core-shell structuring of the cellulose nanofibrils.* Cellulose, 2013. **21**(1): p. 323-333.
7. Larsson, P.A., L.A. Berglund, and L. Wagberg, *Ductile all-cellulose nanocomposite films fabricated from core-shell structured cellulose nanofibrils.* Biomacromolecules, 2014. **15**(6): p. 2218-23.
8. Larsson, P.A. and L. Wågberg, *Towards natural-fibre-based thermoplastic films produced by conventional papermaking.* Green Chemistry, 2016. **18**(11): p. 3324-3333.
9. Linvill, Larsson, and Östlund, *Dynamic Mechanical Thermal Analysis Data of Sheets Made from Wood-Based Cellulose Fibers Partially Converted to Dialcohol Cellulose.* Data Brief, 2017. **14**: p. 504-506.
10. Linvill, E., P.A. Larsson, and S. Östlund, *Advanced three-dimensional paper structures: Mechanical characterization and forming of sheets made from modified cellulose fibers.* Materials & Design, 2017. **128**: p. 231-240.
11. Engel, E.R., G. Lo Re, and P.A. Larsson, *Melt processing of chemically modified cellulosic fibres with only water as plasticiser: Effects of moisture content and processing temperature.* Carbohydrate Polymers, 2025. **348**: p. 122891.
12. Elfaleh, I., et al., *A comprehensive review of natural fibers and their composites: An eco-friendly alternative to conventional materials.* Results in Engineering, 2023. **19**: p. 101271.
13. Zhou, J., et al., *Improving the degree of polymerization of cellulose nanofibers by largely preserving native structure of wood fibers.* Carbohydrate Polymers, 2022. **296**: p. 119919.
14. French, A.D., *Glucose, not cellobiose, is the repeating unit of cellulose and why that is important.* Cellulose, 2017. **24**(11): p. 4605-4609.
15. Kotov, N., et al., *Elucidating the fine-scale structural morphology of nanocellulose by nano infrared spectroscopy.* Carbohydrate Polymers, 2023. **302**: p. 120320.

16. Larsson, P.T., et al., *Interpreting SAXS data recorded on cellulose rich pulps.* Cellulose, 2022. **29**(1): p. 117-131.
17. Isogai, A., T. Saito, and H. Fukuzumi, *TEMPO-oxidized cellulose nanofibers.* Nanoscale, 2011. **3**(1): p. 71-85.
18. Moon, R.J., et al., *Cellulose nanomaterials review: structure, properties and nanocomposites.* Chemical Society Reviews, 2011. **40**(7): p. 3941-3994.
19. Lavoine, N., et al., *Microfibrillated cellulose - its barrier properties and applications in cellulosic materials: a review.* Carbohydr Polym, 2012. **90**(2): p. 735-64.
20. Paajanen, A., et al., *Nanoscale Mechanism of Moisture-Induced Swelling in Wood Microfibril Bundles.* Nano Letters, 2022. **22**(13): p. 5143-5150.
21. Paajanen, A., et al., *Chirality and bound water in the hierarchical cellulose structure.* Cellulose, 2019. **26**(10): p. 5877-5892.
22. Sjöstedt, A., et al., *Structural changes during swelling of highly charged cellulose fibres.* Cellulose, 2015. **22**(5): p. 2943-2953.
23. Sjöström, E., *Chapter 1 - The Structure of Wood*, in *Wood Chemistry (Second Edition)*, E. Sjöström, Editor. 1993, Academic Press: San Diego. p. 1-20.
24. Cave, I.D., *Modelling the structure of the softwood cell wall for computation of mechanical properties.* Wood Science and Technology, 1976. **10**(1): p. 19-28.
25. Cave, I.D. and J.C.F. Walker, *Stiffness of wood in fast-grown plantation softwoods: the influence of microfibril angle.* Forest Products Journal, 1994. **44**: p. 43-48.
26. Reza, M., et al., *Cellulose Elementary Fibrils Assemble into Helical Bundles in S₁ Layer of Spruce Tracheid Wall.* Biomacromolecules, 2017. **18**(2): p. 374-378.
27. Jarvis, M.C., *Structure of native cellulose microfibrils, the starting point for nanocellulose manufacture.* Philosophical Transactions of the Royal Society A: Mathematical, Physical and Engineering Sciences, 2018. **376**(2112): p. 20170045.
28. Plaza, N.Z., et al., *Informing the improvement of forest products durability using small angle neutron scattering.* Cellulose, 2016. **23**(3): p. 1593-1607.
29. De Assis, T., et al., *Comparison of Wood and Non-Wood Market Pulps for Tissue Paper Application.* Bioresources, 2019. **14**: p. 6781-6810.
30. Zeljko, G., *Microfibril Angle in Juvenile, Adult and Compression Wood of Spruce and Silver Fir.* Phyton, Annales Rei Botanicae, Horn, 1999. **93_3**(Plant Physiology): p. 129 -132
31. A, T. and F. Abdul, *Cellulose Microfibril Angle in Wood and Its Dynamic Mechanical Significance.* 2013.
32. Rafsanjani, A., et al., *Hygroscopic swelling and shrinkage of latewood cell wall micropillars reveal ultrastructural anisotropy.* J R Soc Interface, 2014. **11**(95): p. 20140126.

33. Nishiyama, Y., P. Langan, and H. Chanzy, *Crystal structure and hydrogen-bonding system in cellulose Ibeta from synchrotron X-ray and neutron fiber diffraction.* J Am Chem Soc, 2002. **124**(31): p. 9074-82.
34. Nishiyama, Y., et al., *Crystal structure and hydrogen bonding system in cellulose I(alpha) from synchrotron X-ray and neutron fiber diffraction.* J Am Chem Soc, 2003. **125**(47): p. 14300-6.
35. Atalla, R.H. and D.L. VanderHart, *Native Cellulose: A Composite of Two Distinct Crystalline Forms.* Science, 1984. **223**(4633): p. 283-285.
36. Jarvis, M., *Cellulose stacks up.* Nature, 2003. **426**(6967): p. 611-612.
37. Nishiyama, Y., *Structure and properties of the cellulose microfibril.* Journal of Wood Science, 2009. **55**(4): p. 241-249.
38. Kim, D., et al., *In-Depth Understanding of the Effect of the Distribution of Substituents on the Morphology and Physical Properties of Ethylcellulose: Molecular Dynamics Simulations Insights.* Biomacromolecules, 2024. **25**(7): p. 4046-4062.
39. Shen, T. and S. Gnanakaran, *The Stability of Cellulose: A Statistical Perspective from a Coarse-Grained Model of Hydrogen-Bond Networks.* Biophysical Journal, 2009. **96**(8): p. 3032-3040.
40. Valeri, I.K., *Crystalline cellulose: structure and hydrogen bonds.* Russian Chemical Reviews, 2010. **79**(3): p. 231.
41. Wohlert, M., et al., *Cellulose and the role of hydrogen bonds: not in charge of everything.* Cellulose, 2022. **29**(1): p. 1-23.
42. TAPPI, *Fines fraction of paper stock by wet screening. Test method T 261 cm-941994, Britt Jar.* TAPPI 1994.
43. SCAN, *Mechanical and chemical pulps – fines content. Standard CM 66:052005.* SCAN, 2005.
44. Mark, R., *Structure and structural anisotropy. V. Dimensional characterization of shives, slivers, and fines.* Handbook of physical and mechanical testing of paper and paperboard, 1984. **2**.
45. Paavilainen, L., *Importance of particle size-fibre length and fines-for the characterization of softwood kraft pulp.* Paperi ja puu, 1990. **72**(5): p. 516-526.
46. Karnis, A., *Mechanism of fibre development in mechanical pulping.* Journal of Pulp and Paper Science, 1994. **20**(10): p. J280-J288.
47. Luukko, K., *On the characterization of mechanical pulp fines: A review.* Paperi ja Puu/Paper and Timber, 1998. **80**(6): p. 441-448.
48. Brecht, W. and K. Klemm, *Das Strukturgemisch eines Holzschliffes als Schlüssel für die Kenntnis seiner technologischen Eigenschaften.* Wochenbl für Pap, 1952. **80**: p. 364-370.
49. Page, D., *A theory for the tensile strength of paper.* Tappi, 1969. **52**: p. 674-681.
50. Hawes, J.M. and M.R. Doshi. *The contribution of different types of fines to the properties of handsheets made from recycled paper*. in *TAPPI Proceedings 1986 Pulping Conference*. 1986.

51. Sjöstedt, A., *Preparation and characterization of nanoporous cellulose fibres and their use in new material concepts*, in *Department of Fibre and Polymer Technology*. 2014, KTH Royal Institute of Technology: Stockholm, Sweden.
52. Kristiansen, K.A., A. Potthast, and B.E. Christensen, *Periodate oxidation of polysaccharides for modification of chemical and physical properties.* Carbohydrate Research, 2010. **345**(10): p. 1264-1271.
53. Börjesson, M., et al., *Periodate oxidation of xylan-based hemicelluloses and its effect on their thermal properties.* Carbohydrate Polymers, 2018. **202**: p. 280-287.
54. Palasingh, C., et al., *Modification of xylan via an oxidation–reduction reaction.* Carbohydrate Polymers, 2022. **292**: p. 119660.
55. Nypelo, T., et al., *Review: Periodate oxidation of wood polysaccharides-Modulation of hierarchies.* Carbohydr Polym, 2021. **252**: p. 117105.
56. Varma, A.J. and V.B. Chavan, *A study of crystallinity changes in oxidised celluloses.* Polymer Degradation and Stability, 1995. **49**(2): p. 245-250.
57. Kim, U.-J., et al., *Periodate Oxidation of Crystalline Cellulose.* Biomacromolecules, 2000. **1**(3): p. 488-492.
58. Potthast, A., et al., *Studies on oxidative modifications of cellulose in the periodate system: Molecular weight distribution and carbonyl group profiles.* 2007. **61**(6): p. 662-667.
59. Aimin, T., et al., *Influence of ultrasound treatment on accessibility and regioselective oxidation reactivity of cellulose.* Ultrasonics Sonochemistry, 2005. **12**(6): p. 467-472.
60. Sirviö, J., et al., *Dialdehyde cellulose microfibers generated from wood pulp by milling-induced periodate oxidation.* Carbohydrate Polymers, 2011. **86**(1): p. 260-265.
61. Sirvio, J., et al., *Periodate oxidation of cellulose at elevated temperatures using metal salts as cellulose activators.* Carbohydrate Polymers, 2011. **83**(3): p. 1293-1297.
62. Sihtola, H., *Chemical properties of modified celluloses.* Die Makromolekulare Chemie, 1960. **35**(1): p. 250-265.
63. López Durán, V., P.A. Larsson, and L. Wågberg, *On the relationship between fibre composition and material properties following periodate oxidation and borohydride reduction of lignocellulosic fibres.* Cellulose, 2016. **23**(6): p. 3495-3510.
64. Lopez Duran, V., P.A. Larsson, and L. Wagberg, *Chemical modification of cellulose-rich fibres to clarify the influence of the chemical structure on the physical and mechanical properties of cellulose fibres and thereof made sheets.* Carbohydr Polym, 2018. **182**: p. 1-7.
65. Mehandzhiyski, A.Y., et al., *Microscopic Insight into the Structure–Processing–Property Relationships of Core–Shell Structured Dialcohol Cellulose Nanoparticles.* ACS Applied Bio Materials, 2022. **5**(10): p. 4793-4802.

66. Han, X., et al., *Planar and uniplanar orientation in nanocellulose films: interpretation of 2D diffraction patterns step-by-step.* Cellulose, 2023. **30**(13): p. 8151-8159.
67. Penttilä, P.A., et al., *Small-angle scattering model for efficient characterization of wood nanostructure and moisture behaviour.* Journal of Applied Crystallography, 2019. **52**(2): p. 369-377.
68. Jakob, H.F., S.E. Tschegg, and P. Fratzl, *Hydration Dependence of the Wood-Cell Wall Structure in Picea abies. A Small-Angle X-ray Scattering Study.* Macromolecules, 1996. **29**(26): p. 8435-8440.
69. Guinier, A., *Small-Angle Scattering of x-rays*. 1955, United States of America: John Wiley & Sons, Inc.
70. Zhao, H. and N.D. Heindel, *Determination of Degree of Substitution of Formyl Groups in Polyaldehyde Dextran by the Hydroxylamine Hydrochloride Method.* Pharmaceutical Research, 1991. **8**(3): p. 400-402.
71. Karlsson, H., et al., *Dynamic nuclear polarization solid-state NMR spectroscopy as a tool to rapidly determine degree of modification in dialcohol cellulose.* Cellulose, 2024.
72. Penttilä, P.A., A. Paajanen, and J.A. Ketoja, *Combining scattering analysis and atomistic simulation of wood-water interactions.* Carbohydrate Polymers, 2021. **251**: p. 117064.
73. Walenta, E., *Small angle x-ray scattering.* Acta Polymerica, 1955. **36**(5): p. 296-296.
74. Teixeira, J., *Small-angle scattering by fractal systems.* Journal of Applied Crystallography, 1988. **21**(6): p. 781-785.
75. Hammouda, B., *Analysis of the Beaucage model.* Journal of Applied Crystallography, 2010. **43**.
76. Schmidt, P.W., *Small-angle scattering studies of disordered, porous and fractal systems.* Journal of Applied Crystallography, 1991. **24**(5): p. 414-435.
77. Forsström, J., B. Andreasson, and L. Wågberg, *Influence of pore structure and water retaining ability of fibres on the strength of papers from unbleached kraft fibres.* 2005. **20**(2): p. 176-185.
78. Sim, G., *Structure of swollen carboxylated cellulose fibers.* Cellulose, 2014. **v. 21**(no. 6): p. pp. 4595-4606-2014 v.21 no.6.
79. Lo Re, G., et al., *Melt Processable Cellulose Fibres Engineered for Replacing Oil-Based Thermoplastics.* SSRN Electronic Journal, 2022.
80. J.E.Stone, *The Effect of Component Removal Upon the Porour Structure of the Cell Wall of Wood.* Pulp and Paper Magazine of Canada, 1968: p. 69 - 74.